

UNIVERSITÀ DEGLI STUDI DI NAPOLI “FEDERICO II”

FACOLTÀ DI INGEGNERIA

TESI DI DOTTORATO DI RICERCA
IN
INGEGNERIA AEROSPAZIALE, NAVALE E DELLA QUALITÀ
XX CICLO

A SIMULATION MODEL FOR TRAJECTORY
FORECAST, PERFORMANCE ANALYSIS AND
AEROSPACE MISSION PLANNING WITH
HIGH ALTITUDE ZERO PRESSURE BALLOONS

RELATORI
Ch.mo Prof. Michele Grassi
Ing. Federico Corrado

CANDIDATO
Ing. Roberto Palumbo

COORDINATORE DEL CORSO DI DOTTORATO
Ch.mo Prof. Antonio Moccia

NOVEMBRE 2007

Table of Contents

Table of Contents	ii
Nomenclature	v
1. Introduction	1
1.1 Scientific Ballooning and its Applications	1
<i>1.1.1 Some History</i>	2
<i>1.1.2 Scientific Balloons</i>	4
1.2 Scientific Ballooning Around the World	6
1.3 Zero-Pressure Balloons	7
1.4 Objective of this work	10
2. The PRORA-USV Project	11
2.1 Project Overview	11
2.2 The Missions	13
2.3 The DTFT1 Mission	14
3. ACHAB: Analysis Code for High Altitude Balloons	18
3.1 Balloon Trajectory Models	18
<i>3.1.1 Overview</i>	19
3.2 ACHAB: Analysis Code for High Altitude Balloons	21
3.2.1 Dynamical Model	21
<i>3.2.1.1 Forces</i>	21
<i>3.2.1.2 Aerodynamic Drag Coefficient</i>	23
<i>3.2.1.3 Equations of Motion</i>	24
3.2.2 Geometric Model	25
3.2.3 Thermal Model	28
<i>3.2.3.1 Date and Time of Launch and Solar Elevation Angle</i>	30
<i>3.2.3.2 Atmospheric Transmissivity</i>	33
<i>3.2.3.3 Direct Solar Environment</i>	34
<i>3.2.3.4 Thermal Infrared Environment</i>	36
<i>3.2.3.5 Albedo Environment</i>	36

3.2.3.6 Convective Heat Transfer	37
3.2.4 Heat Loads	40
3.2.4.1 Film Optical Properties	40
3.2.4.2 Heat Loads	42
3.2.5 Heat Transfer Differential Equations	44
3.2.6 Valve and Duct Flow Differential Equations	45
3.2.7 Ballasting	47
3.2.8 Closing Remarks	47
4. ACHAB at Work	48
4.1 ACHAB Simulation Environment	48
4.2 Input Data	49
4.2.1 Balloon Characteristics	49
4.2.1.1 Mass and Volume Properties	49
4.2.1.2 Geometric Characteristics of Ducts and Valves	51
4.2.1.3 Film Radiative Properties	52
4.2.1.4 Aerodynamic Drag Coefficient	53
4.2.2 Location, Date and Time of Launch	54
4.2.3 Ballasting	54
4.2.4 Thermodynamic Data	55
4.2.5 Atmospheric Data	56
4.2.6 Albedo Factor	57
4.2.7 Initial Data	57
4.2.8 Initial Gas Mass and Free Lift	58
4.3 Illustrative Simulation: Results	59
5. Validation of the Code	64
5.1 Validation Procedure	64
5.1.1 A note about SINBAD	65
5.2 Case 1 – HASI 2003 Balloon Flight	66
5.2.1 Advantages and Limitations of the Available Flight Data	66
5.2.2 Input Data	67
5.2.3 Results	67
5.3 Case 2 – ARD 1995 Balloon Flight Test	71
5.3.1 Advantages and Limitations of the Available Flight Data	71
5.3.2 Input Data	72
5.3.3 Results	73
5.4 Validation Results	76

6. The USV-DTFT1 Balloon Flight	78
6.1 Mission Planning	78
<i>6.1.1 Determining the Flight Envelope</i>	<i>79</i>
6.2 Flight Analysis and Results	80
<i>6.2.1 Input Data</i>	<i>81</i>
<i>6.2.2 Prediction Performance at -18 hours before Launch</i>	<i>81</i>
<i>6.2.3 Post-Flight Analysis Performance</i>	<i>83</i>
6.3 Final Considerations	88
7. Lessons Learned from the USV-DTFT1 Mission	90
7.1 Lessons Learned	90
7.2 Effects of Clouds on Thermal Fluxes	92
8. ACHAB Related Projects	94
8.1 ACHAB Related Projects	94
8.2 SANBA: The Balloon Navigation Facility	95
8.3 Balloon Mission Optimization Facility	97
8.4 Other Applications	99
9. Conclusions and Future Work	100
9.1 Conclusions	100
9.2 Future Work	102
Acknowledgments	103
References	104

Nomenclature

ACHAB	Analysis Code for High-Altitude Balloons	
<i>Albedo</i>	Albedo coefficient	
<i>Albedo</i> _{ClearSky}	Albedo coefficient in clear-sky conditions	
<i>Albedo</i> _{Cloud}	Albedo coefficient of the cloud layer	
A_{duct}	Cross sectional area of the venting ducts	[m ²]
A_{valve}	Cross sectional area of the gas valves	[m ²]
ASI	Agenzia Spaziale Italiana (Italian Space Agency)	
CIRA	Centro Italiano Ricerche Aerospaziali	
C_d	Balloon drag coefficient	
$C'_{discharge}$	Discharge coefficient of the venting ducts	
$C''_{discharge}$	Discharge coefficient of the valves	
CF	Cloud cover fraction	
CNMCA	Centro Nazionale di Meteorologia e Climatologia Aeronautica	
c_f	Specific heat of the film material	[J/kg/K]
c_v	Specific heat at constant volume of the lifting gas	(for Helium: 3121.5 J/kg/K)
C_{added}	Added mass coefficient	
DTFT	Drop Transonic Flight Test	
e	Orbital eccentricity	
ECMWF	European Centre for Medium-Range Weather Forecasts	
ELV	Solar elevation angle above the true horizon	[rad]
FDR	Flight Data Recorder file	
Fr	Froude Number	
FTB	Flight Test Bed	
g	Acceleration of gravity	[m/s ²]
JD	Julian Date	[days]
k_{ball}	Ballast discharge rate	[kg/min]
Lat	Latitude	[deg]
$Long$	Longitude	[deg]
$L_{goreDesign}$	Maximum gore length	[m]
LTA	Lighter-than-air	

M_{film}	Mass of balloon film	[kg]
M_{gas}	Mass of balloon gas	[kg]
M_{load}	Mass of payload	[kg]
$M_{ballast}$	Total ballast	[kg]
MW_{air}	Molecular weight of dry Air: 28.9644	[g/mol]
MW_{gas}	Molecular weight of lifting gas: Helium: 4.002602	[g/mol]
p_{air}	Ambient pressure	[Pa]
p_0	Air pressure at sea level	[Pa]
p_{gas}	Lifting Gas (Helium) pressure	[Pa]
PRORA	Programma Nazionale Ricerca Aerospaziale	
q_{Albedo}	Diffuse planetary albedo flux	[W/m ²]
q_{Sun}	Direct solar flux	[W/m ²]
$q_{IREarth}$	Diffuse planetary longwave flux (Earth)	[W/m ²]
R_{AU}	Mean orbital radius	[AU]
R_{Earth}	Earth radius	[m]
R_{air}	Specific gas constant of Air	(287.05 J/kg/K)
R_{gas}	Specific gas constant of the lifting gas	(for Helium: 2078.5 J/kg/K)
Re	Reynolds Number	
ρ_{air}	Air density	[kg/m ³]
ρ_{gas}	Lifting Gas (Helium) density	[kg/m ³]
RLV	Reusable Launch Vehicle	
RoC	Rate of Climb	[m/s]
SANBA	System for Augmented Navigation for BALloon Missions	
SINBAD	Scientific Balloon Analysis Model	
T_{air}	Air Temperature	[K]
T_{film}	Balloon film bulk temperature	[K]
T_{gas}	Lifting Gas (Helium) Temperature	[K]
USV	Unmanned Space Vehicle	
UT	Universal Time	
$V_{x,y,z}$	Inertial velocity components	[m/s]
$V_{wind\ x}$	Wind velocity components	[m/s]
$Volume$	Balloon volume	[m ³]
$Volume_{Design}$	Maximum design volume of the balloon	[m ³]
Γ	Flight-path angle	[rad]
σ	Stephan-Boltzmann constant, 5.67e-8	[W/m ² /K ⁴]

γ	Specific heats ratio, c_p/c_v
α	Averaged balloon film absorptivity, visible spectrum
α_{IR}	Averaged balloon film absorptivity, IR
ε	Averaged balloon film emissivity
τ	Averaged balloon film transmissivity, visible spectrum
τ_{IR}	Averaged balloon film transmissivity, IR
r	Averaged balloon film reflectivity

1

Introduction

This chapter presents an introduction to scientific ballooning and a brief overview of its applications for science and research. Particular attention is eventually given to zero-pressure balloons as they are the main subject of the present work.

1.1 – Scientific Ballooning and its Applications

A balloon is an unpowered lighter-than-air vehicle (aerostat). Its ability to fly derives from the *principles of buoyancy*. When a body is immersed in a static fluid it experiences an upward force (i.e. opposite to the force of gravity) due to the pressure difference of fluid between the top and the bottom of the body itself. The upward buoyancy force is equal to the magnitude of the weight of fluid displaced by the body. This statement is generally referred to as the Archimedes' Principle, after the

Greek philosopher Archimedes (287 BC – 212 BC) who was the first to observe and describe this phenomenon.

There are essentially two *practical* methods of producing a buoyant aircraft. If the air inside a suitably large and lightweight envelope is heated to a high temperature, the gas (air) expands and a sufficient amount of fluid may be forced out of the interior so that its weight decreases and the total weight of the craft becomes less than the amount of air displaced¹ (hot air balloon).

The other means of achieving buoyant flight is to fill the envelope with a gas that is sufficiently lighter than air¹ (gas balloon).

Although theoretically any gas with a molecular weight lower than that of air would be capable of producing lift, *scientific ballooning* usually takes advantage of the high lifting capacity of helium or hydrogen because of their very low molecular weight. Hydrogen, despite being cost-effective and extremely light, is highly inflammable and therefore its use is usually avoided, especially for manned applications. Ammonia and methane have also sometimes been used for (small) balloons but their limited lift capacity together with their hazardous properties (toxicity and flammability, respectively), have made their use rather uncommon.

Therefore **helium**, although expensive, is the most preferred lifting gas for scientific ballooning applications: indeed it is both light and inert.

1.1.1 – Some History

Balloons are not new vehicles. They all still rely on the two concepts both flown for the first time in 1783 in France: the hot air balloon by the Joseph and Jacques Montgolfier and the hydrogen gas balloon by Jacques Charles and Nicolas Robert. For about a century, these balloons were used primarily for spectacular events during celebrations and were used little for science. The first observations of scientific interest were those of Robertson in 1803 and of Gay-Lussac and Biot in 1804^{2,4}. They demonstrated the decrease of temperature, pressure, and moisture with height and the constant composition of air up to an altitude of 7000 meters^{1,2}.

The first regular series of unmanned ascents for studying the upper atmosphere was launched by Hermite and Besançon in 1892 in France; they started the systematic use of meteorological instruments onboard, in order to sound the atmosphere². Thanks to this kind of effort, the *stratosphere* was discovered in 1898.

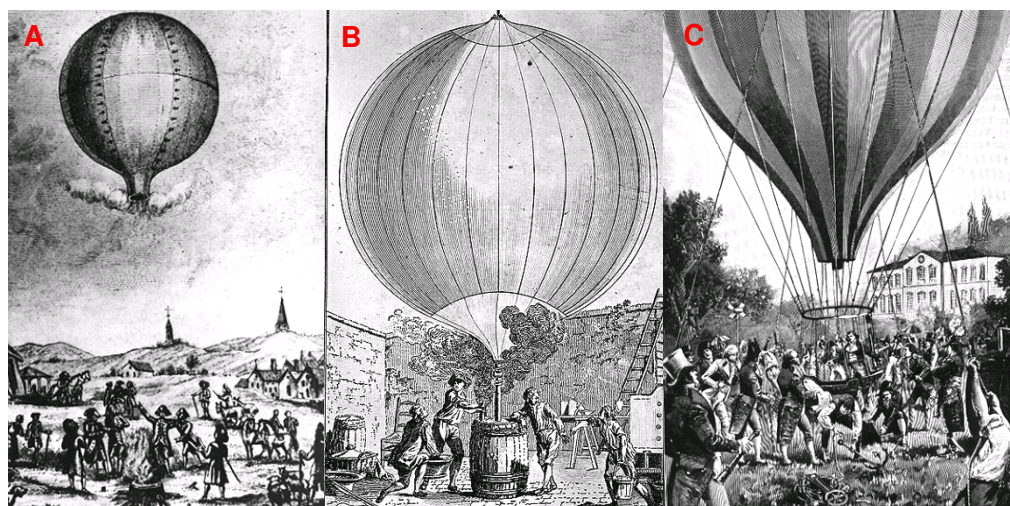


Figure 1.1 – A. The first hot-air balloon flight by the Montgolfier brothers in 1783. B. The first hydrogen balloon in 1783. C. The scientific flight of Gay-Lussac and Biot in 1804 (Images: Ref. 1).

Further improvements to balloon systems were slowly given by the technological progress, but the major breakthrough in atmospheric sciences was the invention of the *radiosonde* by Idrac and Bureau in 1929, who added a radio transmitter to send the temperature, pressure, humidity, and wind information in real time, thus eliminating the need to wait for an unpredictable and sometimes very long recovery of the probes². However, the use of balloons for science other than meteorology remained limited until the arrival in 1947 of plastic film developed by Otto Winzen at General Mills in the United States^{2,5}. The use of *polyethylene resin* for plastic balloons allowed the attainment of higher altitudes and the possibility to carry heavier payloads. Henceforth, a variety of balloons were progressively made available to scientists, and ranged from zero-pressure balloons carrying heavy payloads for a few hours at high altitude to long duration balloons lasting for a few weeks or months in the lower atmosphere². Though their performances and uses varies, they all follow the same physical principles.

Modern scientific ballooning started by the late 1950s in the United States at the University of Minneapolis, later transferring to the *National Center for Atmospheric Research*, NCAR, and then to the *National Aeronautics and Space Administration*, NASA. Soon after, scientific ballooning activities were also started in France at the *Centre National de la Recherche Scientifique*, CNRS, later transferring to the *Centre National d'Etudes Spatiales*, CNES². The balloon technology then propagated rapidly in the 1960s and 1970s to the Soviet Union, Japan, India, Italy, Brazil, and Argentina.

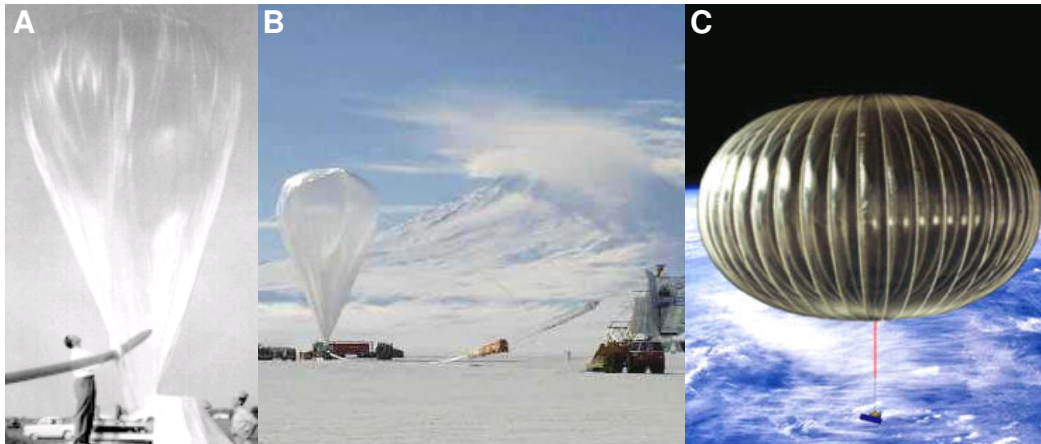


Figure 1.2 – A. One of the first Winzen balloons. B. Boomerang experiment at launch in Antarctica in 2000. C. NASA's Ultra-Long Duration Balloon Concept (Images from Ref. 5, 6).

Today, balloons can be over 500000 cubic meters in volume and can carry scientific payloads that weigh 3000 kg to altitudes higher than 30 km^{2,5,6}. They are certainly a less expensive way to launch and test payloads into a near-space environment. Further details on scientific balloons will be given in the following sections.

1.1.2 – Scientific Balloons

Scientific balloons are very large flexible structures (up to a volume of over 1 million cubic meters) that are designed to carry payloads to the upper layers of the atmosphere. Figure 1.3 shows the typical scientific balloon configuration.



Figure 1.3 – Usual scientific balloon flight chain configuration (Image from Ref. 3).

Balloon systems usually consist of a balloon envelope (see letter A in Figure 1.3), a flight chain (B, C), and a scientific payload (D). The flight chain usually consists of a parachute (B) that allows the entire unit to descend safely when needed, and a gondola (C) that serves as interface between the payload and the balloon and is equipped with communication instruments that enable to track the balloon during its flight.

Scientific balloons can lift payloads that weigh over 3000 kilograms to float altitudes that can be higher than 35 km with a flight time of hours or days or sometimes even of several weeks according to the balloon type^{2,5,6}.

There are essentially three different concepts of scientific balloons:

- the *zero-pressure* balloon, in which ducts at the base of the balloon film allow a very small pressure differential between the inside and the outside;
- the *super-pressure* balloon, which, on the contrary, is sealed and must withstand high internal pressures when it reaches the float altitude;
- the *infra-red Montgolfier* (MIR)², which is basically a zero-pressure hot-air balloon that takes great advantage of the Earth's thermal radiation (during the night) and of sunlight (during the day) in order to heat the lifting gas (air), thanks to a specifically conceived envelope made of different plastic materials.

Table 1.1 reports typical performances of several kinds of scientific balloons.

Scientific Balloon Type	Volume [m ³]	Payload [kg]	Altitude [km]	Duration
Zero-pressure	5000 to 2000000	50 to 2000	25-40	Hours - Days
Pressurized Sphere	50-600	2-20	12-19	Weeks - Months
Super-pressure Pumpkin	1000000	1000	35	Weeks - Months
IR Montgolfier	45000	60	27 (day) 18 (night)	Weeks - Months

Table 1.1 – Typical performances of scientific balloons (From Ref. 2).

Balloons are commonly used as observation platforms in studying the atmosphere. They are used more frequently than orbital satellites. Indeed, if satellites are unique in providing a global view of the Earth's atmosphere, they also suffer several limitations². For example, meteorological parameters can be observed from satellites with difficulty at stratospheric altitudes.

Balloons have also been used to carry payloads and instruments for scientific purposes in a number of different research areas: astronomy, particle physics, magnetospheric physics, atmospheric sciences and much more.

In addition, balloon flights can be performed *within a shorter time frame* than that required for the development of space projects, thus allowing the rapid checking of new ideas, concepts, instruments for later use in space, or even to test small flight vehicles².








1.2 – Scientific Ballooning Around the World

Scientific ballooning programs are being carried out in many countries around the world. It is beyond the scope of this work to give an exhaustive description of these international programs. However it is important to mention the most active balloon launch bases spread around the world.

Launch bases usually provide complete operation services and engineering support to scientists. This includes everything, from inflation and launching to tracking and recovery of the payload.

There are currently more than a dozen of dedicated launch bases around the world operated by the 10 nations that have regular stratospheric balloon projects.

Table 1.2 reports a synthetic overview of the base locations and an estimate of the number of their balloon launches from the start of their activity. These data were collected from Ref. 7.

Continent	Nation	Launch Base Name and Location	Estimated Number of Launches
<i>Europe</i>	<i>France</i>	 Centre de Lancement de Ballons, Aire Sur L'Adour, Landes	300
		 Aeródrome de Gap-Tallard, Haute Alpes	100
	<i>Italy</i>	 Base di Lancio "Luigi Broglio", Trapani-Milo	100
	<i>Norway</i>	 Andoya Rocket Range, Troms	450
	<i>Sweden</i>	 European Space Range (ESRANGE), Kiruna	500
<i>America</i>	<i>Brazil</i>	 Instituto de Pesquisas Meteorológicas, Baurú, Sao Paulo	50
		 Setor de Lançamento de Baloes, Cachoeira Paulista, Sao Paulo	30










	<i>Canada</i>		Scientific Instrumentation Balloon Launch Facility, Vanscoy	90
	<i>USA</i>		Columbia Scientific Balloon Facility, Palestine, TX	1500
			Holloman Air Force Base, Alamogordo, NM	2000
			Fort Sumner Municipal Airport, NM	250
<i>Asia</i>	<i>Japan</i>		Sanriku Balloon Center, Iwate	500
	<i>India</i>		National Balloon Facility, Hyderabad	400
<i>Australian Continent</i>	<i>Australia</i>		Australian Balloon Launch Station, Alice Spring	150
<i>Antarctica</i>	<i>(Japan)</i>		Syowa Station	30
	<i>(USA)</i>		Williams Field, McMurdo Base	60

Table 1.2 – Main balloon launch bases around the world.

This global interest in scientific ballooning makes evident the fact that this kind of approach to scientific research for near-space applications is both *successful* and *cost-effective*. Indeed, as it will be described later, **models and methodologies developed in this work are applied to a particular and quite innovative use of high-altitude balloons as carrier system.**

1.3 – Zero-Pressure Balloons

Zero-pressure balloons are the simplest and most common concept of high-altitude scientific balloon. This section reports a more detailed description of this kind of balloons since they are the main subject of the present work.

Zero-pressure balloons volume varies from 50000 m³ to 2 Mm³ (see Table 1.1), which can carry payloads between 100 kg and 2000 kg (the record is 3600 kg) between 25 and 40km (the record is 42 km)².

In most applications, flight is limited to within the telemetry range from the control station which is usually of 300–400 km (that is for a flight duration of a few hours)². The size of the balloon as well as the weight of the payload, require the use of a mobile crane (or auxiliary balloons) to keep the gondola off the ground during the launch operations, which has to be performed by a well-trained team².

Figure 1.4 shows the main operations and key moments of a typical balloon launch sequence.



Inflation of the balloon.



**Dynamic launch of the balloon.
The payload hangs from a
crane-like device ready to be
released.**



**Lift-off and ascent of the
balloon with payload.**

Figure 1.4 – Typical balloon launch sequence.

As previously said, in zero-pressure balloons, large open ducts at the base of the envelope, vent the excess gas so that the pressure differential from inside to outside remains small (i.e. practically *zero*), thus allowing the attainment of the float altitude. At launch, the balloon is inflated with a certain amount of helium, capable of producing the desired lifting force (*free lift*) and ascent velocity. At lift-off the gas fills only a small fraction of the available volume. Because of the exponential decrease of pressure with altitude, during the ascent, the balloon expands continuously in volume until it reaches its *maximum design volume* attaining the *float altitude*. This float altitude is a function of the balloon design volume, the payload weight, the balloon mass, the lifting gas temperature, and the atmospheric density and temperature.

At float, the gas inside the envelope has completely filled the balloon design volume. Henceforth, since the volume of the balloon ceases to increase, no additional air will be displaced and no further rise in altitude will occur except due to the upward momentum (inertia) of the balloon system⁸. Then, any further increase in gas volume (gas expansion) will, instead, cause the pressure to build up inside the balloon. Once a sufficient amount of pressure is built up inside due to the continued ascent, the balloon loses some of the excess gas through the *venting ducts* into the atmosphere^{2,8}. This continued ascent, due to the upward momentum, results in a reduced air density creating a negative net lift on the balloon which, along with the aerodynamic drag (acting downward), brings the balloon to stop, and consequently, the resulting negative lift causes the balloon to descend. While descending, the downward momentum (inertia) of the balloon system causes the balloon to descend below its equilibrium float altitude, resulting in a higher air density and, therefore, an increase in the lift force⁸. This increase in the lift force along with the upward aerodynamic drag, causes the balloon to stop and reverse its motion, which in turn expands, vents, and reduces the mass of the system. This oscillating cycle continues with decreasing amplitude until the balloon loses all of its excess gas (free lift)^{8,9}.

As a result, in a zero-pressure balloon design, it is very important to properly size the ducts in order to vent the proper amount of gas. Actually, if the balloon over vents it will not even float, whereas under-venting may create the risk of a catastrophic failure due to over pressurization.

For zero-pressure balloon systems, *radiative* and *convective* heat transfers between the balloon and its environment determine the temperature of the buoyant gas. The

temperature of the buoyant gas determines its density and therefore its lifting capacity⁹. Failing to correctly *predict* in-flight gas temperatures can lead to under-filling or over-filling of the balloon at launch. Under-filled systems may not reach the desired float altitude. Overfilled systems may instead burst due to over-pressurization causing the loss of the experiment.

Another important characteristic of zero-pressure balloons is the possibility to control, within certain limits, the vertical speed and altitude of the balloon. Actually by alternatively valving gas and dropping ballast it is possible to change either the balloon's free lift or its *gross mass*^{2,9}. This feature proves to be very useful to attain a particular atmospheric level or to maintain float during day and night transition.

1.4 – Objective of this work

The objective of the present work is to develop a simulation model for trajectory prediction, performance evaluation and aerospace mission planning using high-altitude zero-pressure balloons. This work was carried out in support of the activities concerning the program PRORA-USV by the *Italian Aerospace Research Center* (CIRA) in which the knowledge of balloon systems and of their modeling and simulation is extremely important. In fact, as it will be described in the next chapter, most of the aerospace missions scheduled in the project, are based on a drop of an experimental flight vehicle from a **stratospheric balloon**. Therefore the availability of a tool capable of assessing on the trajectory and on the performance of the balloon flight is of paramount importance in order to meet both mission objectives and safety constraints.

2

The PRORA-USV Project

This chapter gives an overview of the PRORA-USV Project which is being carried out by the *Italian Aerospace Research Center (CIRA)*. As it will be shown, balloon flight is vital to the achievement of the objectives of this program. Indeed mission planning and trajectory prediction for missions related to this specific project were the inspiring reasons for the development of this work.

2.1 – Project Overview

PRORA-USV is a technology development program oriented towards the maturation of certain technologies considered necessary for the timely launch of future generations reusable access-to-space transportation systems^{10,13}. USV (*Unmanned*

Space Vehicles) does not focus on any specific future launcher configuration. Rather it looks at technology advances that are supposed to be fundamental for foreseeable next generations RLVs. The basic belief is that the real revolution in access-to-space cost reduction can be obtained only by pushing the development toward the realization of a today aviation-like system (SSTO-HTHL, sometime called aerospaceplanes)^{10,13}. Identified technological areas requiring innovation and maturation are the following^{10,13}:

- aero-thermal design and optimization of the vehicle configuration, with the main task of improving aerodynamic performances and thermal management, as compared to past and present operational spacecrafts (Soyuz, Space Shuttle);
- development of a fully innovative avionics as well as autonomous guidance navigation and control capability allowing maximum down and cross-range flexibility for a wider family of re-entry trajectories;
- development of hot structures based on innovative architectures and very high performance materials, allowing to withstand the very high temperatures and large thermal loads during the re-entry phase into the atmosphere.

PRORA includes thus technology developments along these three directions up to their validation both on ground using test facilities and in flight using experimental vehicles. Actually the USV program approach consists in the execution of a series of flight tests of increasing complexity, in terms of flight regimes and altitude envelope, with the aim of gradually achieving the final goal of an advanced re-entry capability. For this scope, the design, development and operation of a number of Flying Test Beds (FTBs) represent a relevant effort of the program. The peculiar concept underlying these class of experimental vehicles is that they have to be conceived as *sub-scale unmanned and autonomous flying research laboratories*, allowing them to fly within an enlarged operating envelope rather than a pre-defined and fixed pattern¹⁰⁻¹⁴.

System and technology targets that are needed to achieve the final re-entry capability as above depicted, are grouped in *two major classes of missions* which will be described in the next section.

2.2 – The Missions

The *first class* of missions, covers all of the flight and mission operation issues related to the low atmosphere part of a re-entry pattern, from about 35 km of altitude down to ground, the main focus being on aero-structural and flight control of a re-entry vehicle at transonic and low supersonic speed^{10,11,13,14}. These missions will be accomplished using alternatively the two twin units (*Castore* and *Polluce*) of the FTB_1 laboratory (see Figure 2.1) and using a **stratospheric balloon** as carrier/launch system.



Figure 2.1 – CIRA's FTB_1 experimental vehicle.

Specifically:

- Mission **DTFT1** (Dropped Transonic Flight Test 1, *accomplished on February 24, 2007*)¹² and Mission **DTFT2** (Dropped Transonic Flight Test 2, scheduled for winter 2008) are intended to:
 - validate advanced GNC systems fully developed in house (CIRA) by means of Rapid Prototyping techniques,
 - realize extensive measurements in the field of aerodynamics and structures in order to guarantee proper aero-structural characteristics under transonic and low supersonic conditions
 - validate all of the mission and operation management aspects
- Mission **DSFT** (Dropped Supersonic Flight Test) is intended to validate flight stability, guidance strategies and control laws in supersonic regimes.

The *second class* of missions, will cover all of the flight regimes interested by a complete re-entry pattern, from LEO orbit to landing^{10,11,13,14}. These missions, will be

accomplished with the FTB_X laboratory (see Figure 2.2), using VEGA rocket as reference launch system.



Figure 2.2 – Preliminary concept of the FTB_X experimental vehicle.

Specifically:

- Mission **SRT** (Sub-orbital Re-entry Test) is aimed at performing a partial atmospheric re-entry achieving Mach numbers lower than 10 and minimum acceptable total enthalpy higher than 5 MJ/kg
- Mission **ORT** (Orbital Re-entry Test) will perform a complete re-entry flight from Low Earth Orbit at 200 km achieving Mach numbers lower than 25 and a total enthalpy up to the 25 MJ/kg.

In the next section a more detailed description of the DTFT1 mission will be reported, since the present work was developed in support of the activities concerning the **balloon flight** which plays a crucial role in the accomplishment of the mission.

2.2 – The DTFT1 Mission

The DTFT1 Mission¹², performed on February 24, 2007 from the airport of Tortoli-Arbatax in Sardinia, Italy, was intended to:

- validate advanced GNC systems **fully developed by CIRA** by means of Rapid Prototyping techniques,
- realize extensive measurements in the field of aerodynamics and structures under transonic and low supersonic conditions
- validate all the mission and operation management aspects.

In order to achieve these objectives the FTB_1 vehicle had to autonomously track a predefined longitudinal trajectory.

More in details the mission can be schematically described as follows¹¹:

1. the FTB_1 vehicle (*Castore*) is carried to the launch site and poised for launch under the balloon gondola;
2. the **stratospheric balloon** is *dynamically* launched;

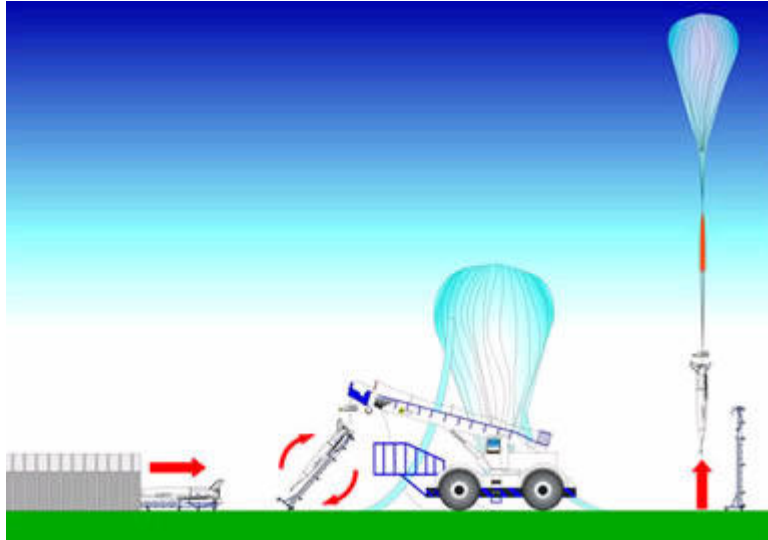


Figure 2.3 – Schematic illustration of the FTB_1 experimental vehicle launch sequence (Ref. 11).

3. the **stratospheric balloon** carries the vehicle to an altitude of about 20 km inside a safe *Release Zone*¹⁵;

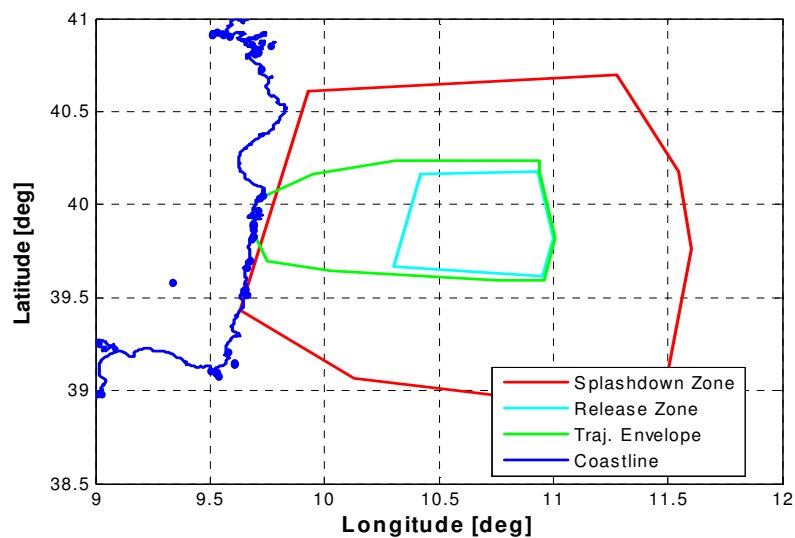


Figure 2.4 – Safety areas outside the coast of Sardinia.

4. the vehicle is released from the gondola;
5. the vehicle performs a longitudinal maneuver in order to track a *constant angle of attack* higher than 4 deg at transonic speeds (Mach numbers between 0.7 and 1.1);
6. the trajectory ends at $Mach \cong 0.6$ (after the transonic phase), when the recovery system is activated.

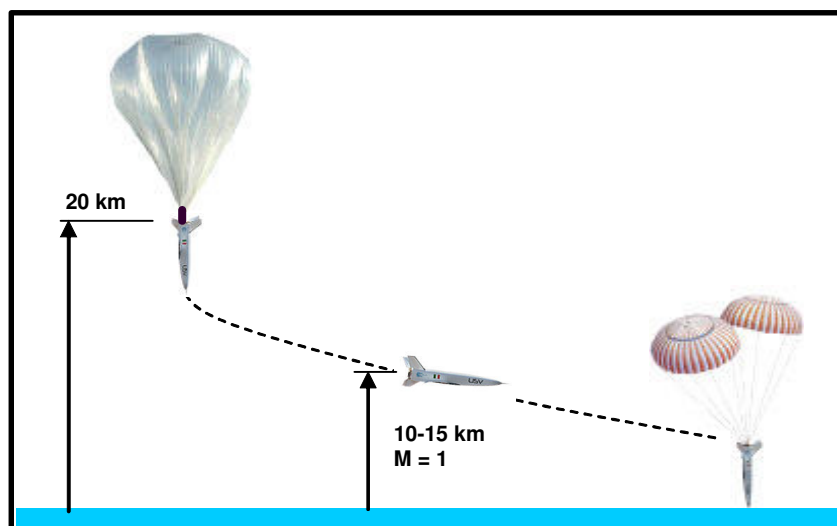


Figure 2.5 – Schematic illustration of the DTFT1 mission profile.

As said at the beginning, the DTFT1 Mission was successfully accomplished during the winter of 2007. Indeed *most* of the mission objectives were achieved¹²:

- the **stratospheric balloon flight was nominal**
- the *expected* control system functionalities of the vehicle were *achieved*, confirming CIRA's ability of developing an advanced GNC system via rapid prototyping techniques.
- aerodynamic and aerostructural experiments were fulfilled (transonic Mach numbers at constant angle of attack were attained).

Unfortunately the reusability of the vehicle could not be demonstrated because the vehicle was highly damaged upon violent impact with water, due to the failure of the recovery system's first stage¹².

It is now clear why *balloon flight* is of vital importance for the accomplishment of the first PRORA-USV missions. Therefore the knowledge of balloon systems and of

their modeling and simulation is extremely important for trajectory prediction and mission planning.

Indeed, as stated in Chapter 1, the *objective* of the present work is to develop a simulation model for trajectory prediction, performance evaluation and aerospace mission planning using high-altitude zero-pressure balloons. This work, as it will be described later on, was actually carried out in support of the activities concerning the balloon flight of the DTFT1 Mission (ascent flight planning and trajectory prediction), and used the DTFT1 Mission to experimentally confirm and ultimately validate the performance of the prediction software.

3

ACHAB: Analysis Code for High Altitude Balloons

In this chapter a detailed description of the theoretical development of a simulation model for the trajectory prediction and performance evaluation of high-altitude zero-pressure balloons will be presented.

3.1 – Balloon Trajectory Models

The problem of modeling the dynamical and thermal behavior of high-altitude balloons, although complex and multidisciplinary, is not entirely new. The first systematic approach to this problem started with Kreith and Kreider¹⁶ in the early 1970s, then followed by Carlson and Horn^{17,18} in the early 1980s. Their results converged in the prediction software THERMTRAJ that ultimately became

SINBAD, NASA's Balloon Scientific Analysis Model¹⁹. Although very popular among the scientific ballooning community, SINBAD is rather old and suffers from several limitations, especially when it comes to *mission planning*. For example, it is not capable of simulating three-dimensional trajectories or it uses a 5-point one-dimensional atmospheric model.

In the present work we will describe the theoretical bases and the development process of **ACHAB** (Analysis Code for High-Altitude Balloons), a *new software* tool for the simulation of the dynamical and thermal behavior of high-altitude zero pressure balloons²⁶.

3.1.1 - Overview

The lifting force that allows a balloon to rise derives from Archimedes' Principle. Concisely the lift of a balloon can be expressed as:

$$(\rho_{air} - \rho_{gas}) \cdot Volume = M_{gross} (1 + f)$$

where *Volume* is the volume, ρ_{air} the density of air and ρ_{gas} that of the lifting gas (helium), M_{gross} the sum of solid masses (balloon envelope and payload), and *f* the free lift. Getting off the ground requires a positive free lift (or excess gas) of generally 10–20%^{2,9}.

During its flight, the balloon can be considered as a thermal and dynamical system that is practically in free evolution inside a complex thermal environment and subject to atmospheric winds. Therefore careful modeling of the thermal effects is of fundamental importance for the correct simulation of the vertical speed of the balloon.

Before delving into the details of the model, it is instructive to give a schematic overview of how the code works. Figure 3.1 shows an illustrative block diagram describing the structure of ACHAB.

Buoyancy, which is the most important force to be determined, is related to the other forces that act on the balloon through a **dynamical model**. The dynamical model, though, needs information that can only be given if a **geometric model** and a **thermal model** are introduced. The geometric model gives a geometric description

of the balloon system (reference areas, incidence areas) while the thermal model takes into account the thermodynamic processes and quantities (gas temperature variation, gas density, balloon film temperature variation, etc). Moreover an **atmospheric model** – which is an input to the code - must also be taken into account to supply air temperature and pressure and information on wind components. The dynamical model, the geometric model, the thermal model and the atmospheric data work together in order to determine, essentially, the volume and the temperature of the lifting gas. These important quantities are then finally used for the computation of buoyancy.

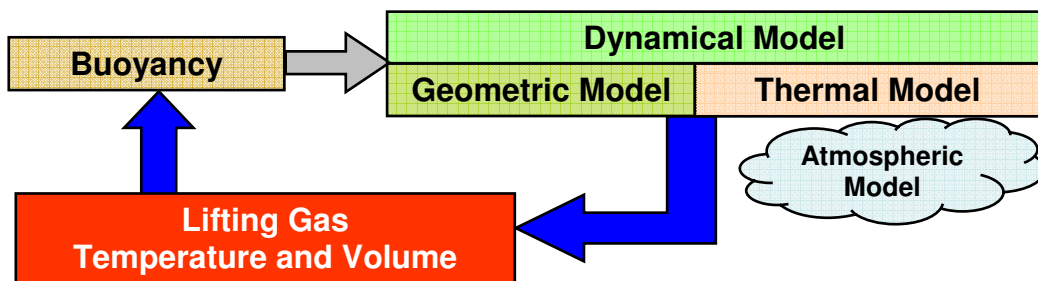


Figure 3.1 – Block diagram describing the logical structure of ACHAB.

At this point, before describing the model, some basic **assumptions** must be made. These assumptions are those classically made when dealing with balloon systems, as far as trajectory prediction is concerned^{9,16,17,18,20}:

- The balloon is considered a 3 degree-of-freedom point mass.
- The variation of g (acceleration of gravity) over the height of a balloon is ignored.
- Lifting gas and air are assumed to follow the perfect gas law.
- Effects of humidity on atmospheric pressure are neglected.
- Lifting gas density and pressure are considered uniform inside the balloon (**except** when considering *valving* or *venting*)
- Lifting gas is transparent, so it does not absorb nor emits.
- Lifting gas temperature is uniform inside the balloon volume.
- Balloon film temperature is uniform along the surface.

3.2 – ACHAB: Analysis Code for High-Altitude Balloons

The development of this model is essentially based on many results given in Ref. 9, Ref. 16, Ref. 17, Ref. 18, Ref. 20, Ref. 22, Ref. 26. We will start describing the dynamical model then the general geometric properties of the balloon and finally the thermal model.

3.2.1 – Dynamical Model

3.2.1.1 – Forces

In order to write the 3D differential equations that describe the balloon dynamics, it is necessary to identify the forces that act on the system. A rigorous analysis of all the forces to which a balloon system is subjected during inflation, launch, and flight is beyond the scope and needs of this model; however, those of greatest importance for the description of the balloon motion are considered to be^{9,16,17,20}:

- net buoyancy
- weight
- aerodynamic drag

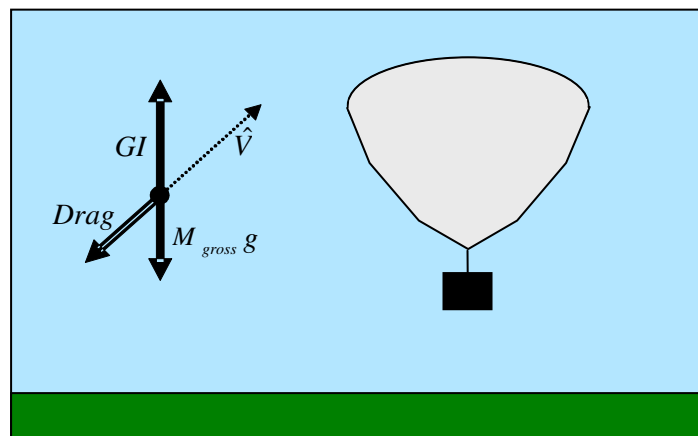


Figure 3.2 – Forces acting on the balloon.

Figure 3.2 shows the forces acting on the balloon. The velocity vector is not oriented vertically because the model is 3-dimensional and takes into account wind disturbances.

Buoyancy force comes from Archimedes' Principle and can be written as:

$$F_{Arch} = g \cdot \rho_{air} \cdot Volume$$

The total **net buoyant force** produced by the balloon is usually defined as the *gross inflation*, GI and is given by:

$$GI = F_{Arch} - M_{gas} g = g(\rho_{air} - \rho_{gas}) \cdot Volume$$

At first, of course, volume must be determined using sea-level values/initial values for pressure, temperature and density (for both air and helium) in the perfect gas law:

$$Volume = M_{gas} R_{gas} \frac{T_{gas}}{P_{gas}}$$

Subsequently the model evolves updating these variables through the thermal equations, allowing the determination of successive values of the *Volume*.

Weight is given by the following:

$$W = M_{gross} g$$

where the gross mass M_{gross} is the overall mass of the balloon less the gas, i.e. the sum of the payload mass, M_{load} , the ballast, and the mass of the balloon film, M_{film} :

$$M_{gross} = M_{film} + M_{load} + M_{ballast}$$

The mass of Helium instead is considered in the net buoyancy force.

The magnitude of the **Drag** force is given by:

$$Drag = \frac{1}{2} \rho_{air} V_{rel}^2 C_d A_{top}$$

the reference area is the top projected area A_{top} (discussed in the next section). C_d is the drag coefficient. V_{rel} is the magnitude of the wind-relative velocity. In particular, if V_{wind_x} , V_{wind_y} and V_{wind_z} are the wind components:

$$V_{rel_x} = V_x - V_{wind_x}$$

$$V_{rel_y} = V_y - V_{wind_y}$$

$$V_{rel_z} = V_z - V_{wind_z}$$

and obviously:

$$V_{rel} = \sqrt{V_{rel_x}^2 + V_{rel_y}^2 + V_{rel_z}^2}$$

3.2.1.2 – Aerodynamic Drag Coefficient

According to Ref. 24, which presents an extended literature survey on drag coefficient models for natural shape balloons, it should be reasonable to consider a variable drag coefficient during the ascent portion of the balloon flight. The arguments supporting this conclusion are essentially three:

1. inconstant shape
2. shape deformability
3. dimensional reasoning

These arguments, according to Ref. 24, explain why the drag coefficient cannot be exclusively dependent of the Reynolds number, but it should also be a function of the Froude number and of another dimensionless parameter that accounts for the shape variations:

$$C_d = f(Re, Fr, L)$$

Indeed a zero-pressure balloon experiences a remarkable shape variation from lift-off to the attainment of the float altitude and consequently it appears reasonable that the drag coefficient should be considered variable.

As a result in this model it is *suggested* the following relationship for the drag coefficient²⁶:

$$C_d = 0.2 \frac{k}{Fr} \cdot \left(\frac{k_1}{Re} + k_2 Re \right) \frac{A_{top}}{A_{top0}}$$

This relationship – with appropriate constants and with an upper saturation value of 1.6 (Ref. 25) – has been found to be quite suitable to fit the flight data at least up to the tropopause where drag effects are more significant than radiative thermal effects²⁶.

This characteristic is a peculiar aspect of ACHAB. Other codes have usually considered a constant drag coefficient, based on the fact that the balloon can be seen as a sphere. Even though we believe that a variable C_d is more appropriate, ACHAB can as well consider a constant coefficient for the computation of the drag force.

3.2.1.3 – Equations of Motion

Now it is possible to write the equations of motion of the balloon. The equations are written in local NED (North – East – Down) reference frame.

The differential equation governing the vertical motion is the following:

$$\ddot{z} = \frac{M_{gross} g - GI + Drag_z}{M_{total}}$$

This equation does not include the momentum variation due to mass loss (i.e. during ballasting and/or valving and/or venting). This effect will be estimated and possibly added in future enhancements of this model.

The total mass, M_{total} , is the sum of the gross mass, the gas mass and the *added* mass:

$$M_{total} = M_{gross} + M_{gas} + C_{added} (\rho_{air} Volume)$$

The *added* mass term takes into account the mass of air that is necessarily dragged along with the balloon during ascent. It is shown in fluid dynamics that if a solid body is immersed in a fluid and is then accelerated, pressures are generated that affect the fluid field to infinity. This creates kinetic energy in the fluid. One can define an effective mass of fluid accelerating with the body: this is called *added mass*²³.

This added mass can be assumed as a fraction of the mass of the fluid displaced. The C_{added} coefficient can range between 0.25 and 0.5 or more²⁰.

Since no force acts horizontally except for the aerodynamic drag (in the presence of winds), the horizontal motion equations are simply:

$$\ddot{x} = \frac{Drag_x}{M_{total}}$$

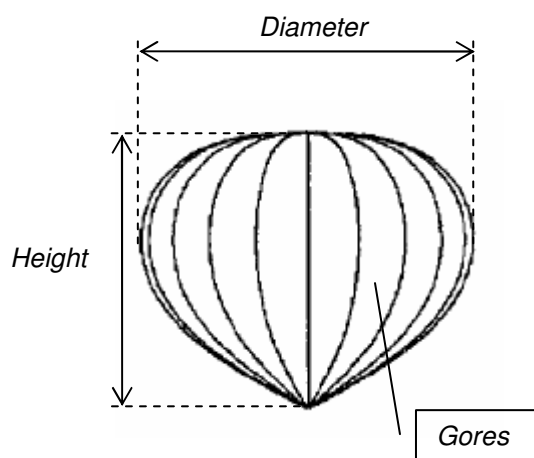
$$\ddot{y} = \frac{Drag_y}{M_{total}}$$

Of course it is now necessary to introduce a geometric model and thermal model to account for variations in the net buoyancy force, balloon volume, drag force and gas mass.

3.2.2 – Geometric Model

The knowledge of the geometric properties of the balloon is essential for the correct modeling of forces and heat loads that act on the balloon.

According to Ref. 20 the geometric properties of a zero-pressure natural shape balloon can be approximated by the following equations:



Balloon diameter, top view, in meters:

$$Diameter = 1.383 \cdot Volume^{\frac{1}{3}}$$

The length of the gore:

$$L_{gore\ B} = 1.914 \cdot Volume^{\frac{1}{3}}$$

The height of a zero-pressure shape:

$$Height = 0.748 \cdot Diameter$$

Surface area showing in a zero pressure shape:

$$A_{surf} \cong 4.94 \cdot Volume^{\frac{2}{3}}$$

In order to take into account the effect of the crenellated surface area of the balloon and the effective exposed surface for convection calculations:

$$A_{surf_1} = 4.94 \cdot Volume_{design}^{\frac{2}{3}} \cdot \left(1 - \cos \left(\pi \frac{L_{gore\ B}}{L_{gore\ Design}} \right) \right)$$

$$A_{effective} = 0.65A_{surf} + 0.35A_{surf_1}$$

Top projected area in m²:

$$A_{top} = \frac{\pi}{4} \cdot Diameter^2$$

The illuminated projected area of a balloon varies with solar elevation angle *ELV*, and uses the top projected area, A_{top} , as the reference.

The elevation angle is defined as the angle between the direction of the Sun and the true horizon as shown in Figure 3.3.

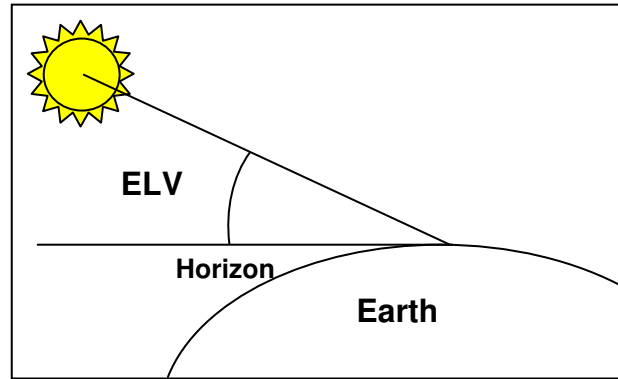


Figure 3.3 – Solar elevation angle.

For a zero-pressure balloon:

$$A_{projected} = A_{top} \cdot [0.9125 + 0.0875 \cos(\pi - 2ELV)]$$

This formulation is consistent with the fact that the projected area for the side-view of a natural shaped balloon is around 82% of the projected area as compared to the top down view²⁷.

In fact if $ELV=0$,

$$A_{projected} = A_{top} \cdot [0.9125 + 0.0875 \cos(\pi)] = A_{top} \cdot 0.825$$

$A_{projected}$ can also be used for the evaluation of the reference surface for drag computation. The basic idea is that A_{top} must be modulated according to the direction of the velocity vector. Therefore we assume the same formula above replacing the ELV angle with the flight-path angle, Γ .

$$A_{projected_{drag}} = A_{top} \cdot [0.9125 + 0.0875 \cos(\pi - 2\Gamma)]$$

3.2.3 – Thermal Model

In order to predict balloon flight performance, it is very important to carefully consider the surrounding thermal environment in which the balloon moves.

The vertical motion of balloons depends critically on the *heat transfer* to and from the gas inside⁹, because the temperature and the density of the gas determine the lift of the balloon. The *balloon film* plays an important role in this heat transfer mechanism, therefore its radiation properties significantly influence the performance and the vertical flight of the balloon.

Before continuing, it is important to state some of the basic assumptions made in developing this thermal model:

- ***Sun Radiation.***

The Sun's spectrum is considered to be approximated by that of a blackbody⁹ at 5550°K.

- ***Earth's Thermal Radiation.***

Earth is considered as a *gray body* with surface temperature T_{ground} and emittance ϵ_{ground} . In addition we will call the energy emitted from the earth-atmosphere system, *thermal infrared radiation*. In fact, even if the Earth emits electromagnetic radiation covering all frequencies, the global mean temperature of the earth-atmosphere system is lower than 300K. As a consequence of *Planck's law* and *Wien's displacement law*, we have that the emissive power of Earth is mainly in the **longwave** window of the electromagnetic spectrum^{29,30}.

- ***Balloon Film Radiation.***

Balloon film is usually at temperatures of about 210-270K. Therefore, it will be considered that as a gray body that emits primarily in the longwave window of the electromagnetic spectrum^{9,29,30}.

The **heat sources** taken into account in this model are the following^{9,18,20,21,27,28}:

- Direct Sun radiation
- Albedo

- Diffuse longwave radiation from ground/atmosphere
- Internal longwave self-glow of heat energy between different patches of the interior skin
- External and internal convection

In the case of nighttime flights, the heat sources to be taken into account are, of course, only the following:

- Diffuse longwave radiation from ground/atmosphere
- Internal longwave self-glow of heat energy between different patches of the interior skin
- External and internal convection

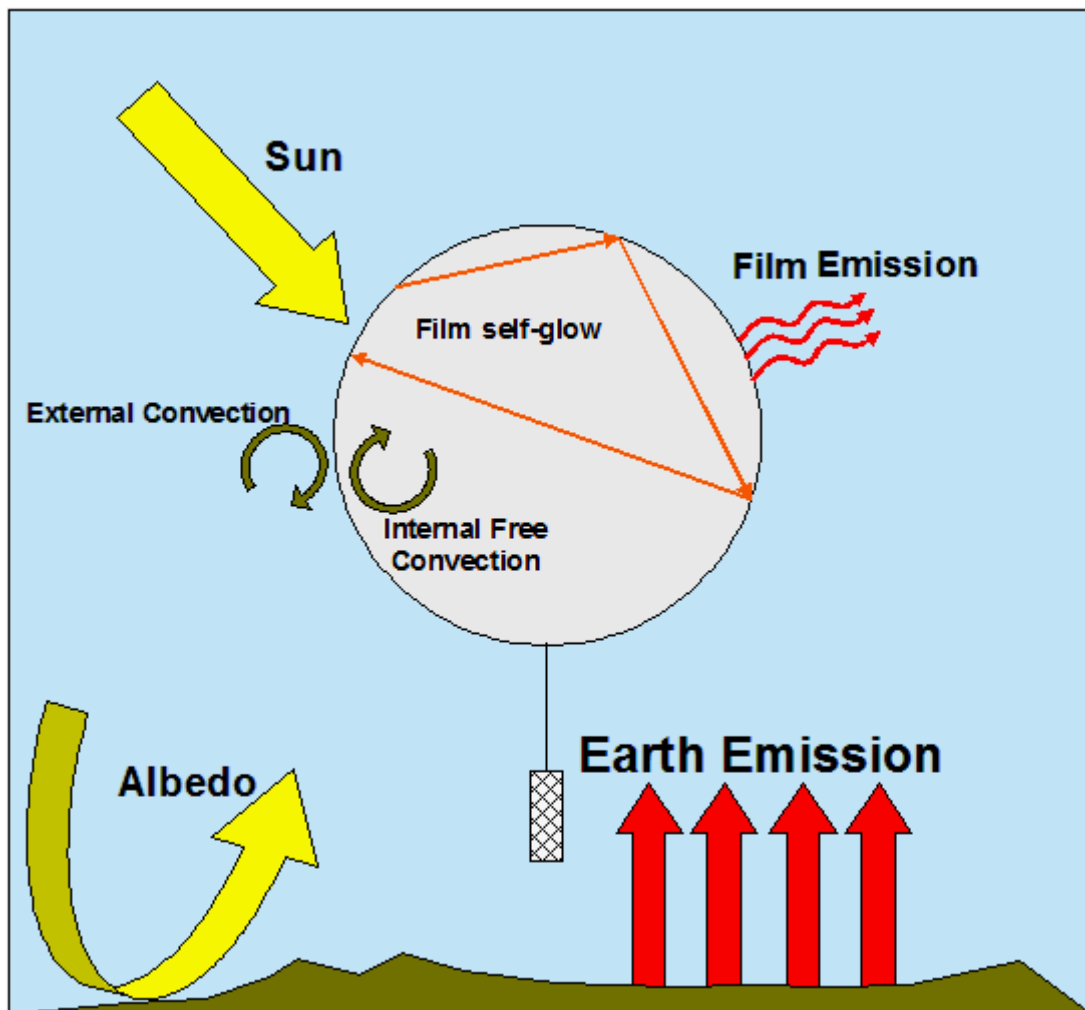


Figure 3.4 – Heat loads acting on the balloon.

These heat sources are considered to be the most important ones that significantly influence the balloon flight. According to Ref. 20 to give an idea of the influences at an altitude of about 33 km on an average sunny day, the fraction of heat loads absorbed in the skin of a large scientific balloon is approximately:

- Planetary surface emission 49%
- Direct Solar 35%
- Albedo 20%
- Internal IR Self-glow 3%
- Atmospheric Convection -7%

Moreover, it is assumed that the lifting gas (helium) is completely **transparent** so it does not emit nor absorb^{9,20}: its temperature may change only as a result of the internal free convection and volume expansion.

In the following subsections each of the heat sources listed above will be described more in details and characterized.

3.2.3.1 – Date and Time of Launch and Solar Elevation Angle

Solar Elevation angle (*ELV*) and its variation during the day is of fundamental importance in computing heat fluxes due to direct solar radiation and albedo. Therefore, according to the date and time of launch and according to the balloon location, solar coordinates must be obtained.

Before computing solar coordinates it is necessary to calculate the Julian Date (*JD*) of the launch. The Julian date is a continuous count of days from 1 January 4713 BC at Greenwich mean noon (= 12h UT).

Conversion of Gregorian calendar date to Julian date for years AD 1801-2099 can be carried out with the following formula³¹:

$$JD = 367K - \left\langle \frac{7 \left(K + \left\langle \frac{(M+9)}{12} \right\rangle \right)}{4} \right\rangle + \left\langle \frac{275M}{9} \right\rangle + I + 17210135 + \frac{UT}{24} - 0.5 \text{sign}(100K + M - 1900025) + 0.5$$

where K is the year ($1801 \leq K \leq 2099$), M is the month ($1 \leq M \leq 12$), I is the day of the month ($1 \leq I \leq 31$), and UT is the universal time in hours. The symbol $\langle \rangle$ indicates the truncation function which extracts the integral part of a number.

To obtain solar coordinates an approximate algorithm can be used. This algorithm computes the Sun's angular coordinates to an accuracy of about 1 arc minute³¹:

- **Convert Local Time to UT .**

Greenwich time can be obtained considering local time zone and daylight saving settings.

- **Compute Julian Date.**

Julian Date is obtained using the formula given above.

- **Compute the number of Julian days and fractions (D) from a reference epoch.**

The reference epoch chosen is JD2000 (January 1, 2000 at 12:00), Julian date 2451545.0.

Therefore:

$$D = JD - 2451545.0$$

where JD is the Julian date of interest.

- **Compute the approximate Sun's geocentric apparent ecliptic longitude.**

An approximate formula is given for the ecliptic longitude:

$$L = q + 1.915 \sin g + 0.020 \sin 2g$$

where g and q are the mean anomaly of the Sun and the mean longitude of the Sun and are given by:

$$g = 357.529 + 0.98560028D$$

$$q = 280.459 + 0.98564736D$$

The Sun's ecliptic latitude, b , can be approximated by $b = 0$. L , g , q and b are in degrees.

- **Convert ecliptic longitude to right ascension RA and declination δ .**

First compute the mean obliquity of the ecliptic, in degrees:

$$e = 23.439 - 0.00000036D$$

Then the Sun's right ascension, RA , and declination, δ , can be obtained from:

$$\tan(RA) = \frac{\cos e \sin L}{\cos L}$$

$$\sin \delta = \sin e \sin L$$

- **Compute sidereal time (in degrees) at Greenwich.**

First compute the number of Julian centuries:

$$T = \frac{D}{36525}$$

Then the sidereal time at Greenwich (in degrees) is given by:

$$\theta_0 = 280.46061837 + 360.98564736629D + 0.000387933T^2 - \frac{T^3}{38710000}$$

- **Convert to local sidereal time.**

Local sidereal time (in degrees) is simply:

$$\theta = \theta_0 + Long$$

where $Long$ is the balloon actual longitude (in degrees).

- **Compute Local Hour Angle (LHA).**

The Local Hour Angle is then:

$$LHA = \theta - RA$$

- **Convert Local Hour Angle and declination to horizon coordinates.**

Now it is possible to compute the local solar elevation angle (*ELV*) and azimuth angle using the following relationships:

$$\sin ELV = \sin(Lat)\sin \delta + \cos(Lat)\cos \delta \cos(LHA)$$

$$\tan AZ = -\frac{\sin(LHA)}{\cos(Lat)\tan \delta - \sin(Lat)\cos(LHA)}$$

where *Lat* is the balloon actual latitude.

Using this algorithm it is possible to simulate the *day and night cycle*.

Twilight.

Before sunrise and again after sunset there are time intervals during which there is natural light provided by the upper atmosphere, which does receive direct sunlight and reflects part of it toward the Earth's surface. This kind of illumination is referred to as twilight.

There are several definitions for twilight according to application. The present model considers **civil twilight**, which is defined to begin (in the morning), and to end (in the evening) when the center of the Sun is geometrically 6 degrees below the horizon³¹.

3.2.3.2 – Atmospheric Transmissivity

Irradiance of both the solar radiation and the longwave radiation is obviously influenced by the presence of the atmosphere. The transmissivity of a solar beam and the attenuation of the ground thermal radiation, follow an exponential decay⁹ based on Beer's Law. All of the following equations are based on those from Ref. 9 and Ref. 20.

The *AirMass* factor is necessary to take into account the air mass that a solar beam crosses while reaching the balloon. It explicitly depends upon the solar elevation angle.

$$AirMass = \left(\frac{P_{air}}{P_0} \right) \left[\sqrt{1229 + (614 \sin(ELV))^2} - 614 \sin(ELV) \right]$$

During twilight, *AirMass* is evaluated considering, $ELV = 0$:

$$AirMass = \left(\frac{P_{air}}{P_0} \right) \sqrt{1229}$$

The atmospheric transmissivity for direct sunlight is then defined:

$$\tau_{atm} = 0.5 \left[e^{-0.65 \cdot AirMass} + e^{-0.095 \cdot AirMass} \right]$$

As with visible light, the ground IR is attenuated with a similar formula:

$$\tau_{atmIR} = 1.716 - 0.5 \cdot \left[e^{-\frac{0.65 P_{air}}{P_0}} + e^{-\frac{0.095 P_{air}}{P_0}} \right]$$

3.2.3.3 – Direct Solar Environment

Over 99% of the solar energy is contained within a narrow wavelength band between 0.2μ and 4μ , and for most engineering heat transfer calculations the Sun's spectrum can be approximated by that of a blackbody at 5550°K . The solar radiation per unit area on a horizontal surface outside the Earth's atmosphere depends only on the *solar constant* and on the solar elevation angle⁹.

Therefore to characterize the solar environment, it is important to know several orbital parameters²⁰.

The following treatment is general and can be applied to any planet with a small orbital eccentricity.

The Mean Anomaly (MA) can be determined as follows:

$$MA = 2\pi \frac{Day_{number}}{DaysPerYear}$$

where $DaysPerYear$ is the total number of days in a year for the considered planet (for Earth = 365) and Day_{number} is the number of the balloon flight day starting from perihelion (for Earth, perihelion occurs on January 2).

The true anomaly (TA) can be approximated by the following equation provided that the orbital eccentricity is small:

$$TA \approx MA + 2e \sin(MA) + \frac{5}{4} e^2 \sin(2MA)$$

The solar irradiance flux at the top of the atmosphere is related to the position of the planet (Earth) along its orbit around the Sun:

$$I_{Sun} = \frac{1367.5}{R_{AU}^2} \left[\frac{1 + e \cos(TA)}{1 - e^2} \right]^2 \quad [\text{W/m}^2]$$

For Earth: $R_{AU} = 1$ and $e = 0.016708$. The constant 1367.5 [W/m²] is the nominal value of the solar constant³².

At the balloon altitude Z , the direct solar irradiance is equal to the product of its value at the top of the atmosphere and the atmospheric transmittance:

$$I_{SunZ} = I_{Sun} \tau_{atm}$$

Thus the direct solar flux acting on the balloon is:

$$q_{Sun} = I_{SunZ} \quad [\text{W/m}^2]$$

3.2.3.4 – Thermal Infrared Environment

The longwave diffuse flux at ground level with ground emissivity ϵ_{ground} and ground temperature T_{ground} can be expressed as:

$$q_{IRground} = \epsilon_{ground} \sigma T_{ground}^4$$

The ground emissivity coefficient ϵ_{ground} strictly depends on the characteristics of the launch/flight site. Ground emissivity is usually low in the hottest places while it is usually high in the coldest ones²⁰. However it is possible to consider an average value: $\epsilon_{ground} = 0.95$. T_{ground} is the equilibrium radiation temperature.

Just as solar radiation is attenuated for the thickness of the atmosphere, the same is applied to the ground thermal emission that has to pass through a certain amount of atmosphere to reach the balloon. Thus the longwave radiation flux from ground at the balloon altitude Z is:

$$q_{IREarth} = q_{IRgroundZ} = q_{IRground} \tau_{atmIR} \quad [\text{W/m}^2]$$

3.2.3.5 – Albedo Environment

There is a simple relationship relating surface albedo and albedo flux²⁰. This relationship involves the solar flux, the albedo coefficient and the solar elevation angle.

$$q_{Albedo} = Albedo \cdot I_{Sun} \cdot \sin(ELV)$$

When $ELV \leq 0$ (night and twilight), it is assumed that $q_{Albedo} = 0$.

The *Albedo* coefficient accounts for the fraction of solar radiation that is reflected by the planet surface and atmosphere. Figure 3.5 (Ref. 9) shows a plot of the *Albedo* coefficient for Earth as a function of latitude in different meteorological conditions.

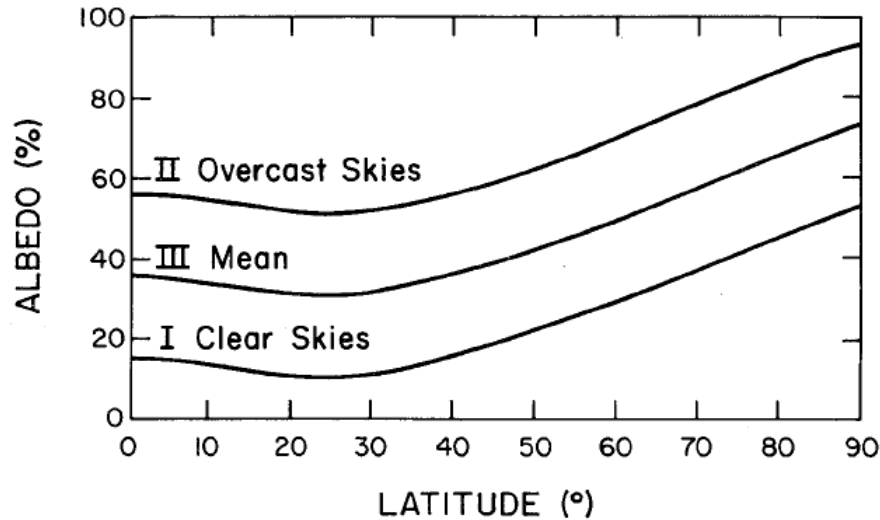


Figure 3.5 – Albedo coefficient as a function of latitude in different meteorological conditions (Taken from Ref. 9).

A typical mean value is 30%. However a more accurate value (depending on the characteristics of the flight zone) must be chosen since the albedo significantly affects the thermal environment.

The albedo has a significant influence on the balloon performance only at high-altitudes and at float. Therefore modifications to albedo due to clouds and/or possible meteorological changes in the upper atmosphere should be taken into account to correctly predict the balloon performance at float altitude.

At the moment the present model considers only a constant albedo factor throughout the entire flight.

3.2.3.6 – Convective Heat Transfer

The convective heat transfer of the balloon involves transfers between the atmosphere and the exterior skin, and between the lifting gas and the interior skin. The external convection is partitioned into free convection and forced convection. In order to determine the convective heat transfer coefficients some properties of air and of helium must be considered^{9,20}:

- Dynamic viscosity of air:

$$\mu_{air} = \frac{1.458 \cdot 10^{-6} \cdot T_{air}^{1.5}}{T_{air} + 110.4}$$

- Dynamic viscosity of Helium:

$$\mu_{gas} = 1.895 \cdot 10^{-5} \cdot \left(\frac{T_{gas}}{273.15} \right)^{0.647}$$

- Conductivity of air:

$$k_{air} = 0.0241 \cdot \left(\frac{T_{air}}{273.15} \right)^{0.9}$$

- Conductivity of Helium:

$$k_{gas} = 0.144 \cdot \left(\frac{T_{gas}}{273.15} \right)^{0.7}$$

- Prandtl Number for air:

$$Pr_{air} = 0.804 - 3.25 \cdot 10^{-4} \cdot T_{air}$$

- Prandtl Number for Helium:

$$Pr_{gas} = 0.729 - 1.6 \cdot 10^{-4} \cdot T_{gas}$$

External Free Convection.

Convection heat transfer coefficients (HC) are usually expressed in terms of the Nusselt number, which is defined in general as:

$$Nu = \frac{HC \cdot L}{k}$$

where HC is the heat transfer coefficient, L a characteristic length and k is the thermal conductivity of the adjacent gas.

For free convection between the external skin and the air the following formulation of the Nusselt number is considered:

$$Nu_{free} = \frac{HC_{free} \text{Diameter}}{k_{air}}$$

Nusselt numbers for free convection problems are usually correlated to Rayleigh numbers. The general form is:

$$Nu = a_0 + a_1 Ra^n$$

where Rayleigh number is the product of the Grashof number and Prandtl number ($Ra = GrPr$), and a_0 , a_1 and n are usually determined experimentally.

The Nusselt number used in this model is taken from Ref. 9, 17, 18, 20. The Grashof number for air Gr_{air} is defined as:

$$Gr_{air} = \frac{\rho_{air}^2 g |T_{film} - T_{air}| \text{Diameter}^3}{T_{air} \mu_{air}^2}$$

External Forced Convection.

This kind of convection depends on the vertical velocity of the balloon that forces the relative movement of air with respect to the external skin.

The formulations of the Nusselt number (Nu_{forced}) for external forced convection used in this model are those reported in Ref. 9, 18, 20.

Hence, this yields to the following coefficient:

$$HC_{forced} = \frac{k_{air}}{\text{Diameter}} Nu_{forced}$$

External Convection.

Finally the actual external convection heat transfer coefficient is chosen to be the greater of the two values between free and forced convection²⁰:

$$HC_{external} = \max(HC_{free}, HC_{forced})$$

Internal Free Convection.

The internal free convection coefficient is taken from Ref. 9, 18, 20. As usual the formulation of the Nusselt number for free convection is:

$$Nu_{IntFree} = a_0 + a_1 Ra_{gas}^n$$

As always, $Ra_{gas} = Gr_{gas} Pr_{gas}$ and:

$$Gr_{gas} = \frac{\rho_{gas}^2 g |T_{film} - T_{gas}| Diameter^3}{T_{gas} \mu_{gas}^2}$$

The internal convection heat transfer coefficient is therefore:

$$HC_{internal} = \frac{k_{gas}}{Diameter} Nu_{IntFree}$$

3.2.4 – Heat Loads

It is now possible to evaluate the heat loads acting on the balloon skin. Figure 3.4 schematically shows the different thermal sources that have been considered in the development of this model.

3.2.4.1 – Film Optical Properties

The optical surface properties of the balloon are expressed as absorptivity α , transmissivity τ , reflectivity r and emissivity ε and are averaged on the total film surface. These coefficients are usually wavelength dependent^{29,30}. In addition while ε

strictly depends on the **surface** characteristics (material or coating) of the balloon film, absorptivity, transmissivity and reflectivity, depend on both the kind of balloon film and the kind of **irradiance**^{29,30}.

We have said earlier that over 99% of the solar energy is contained within a narrow wavelength band between 0.2 μ and 4 μ . Therefore when dealing with solar radiation we will consider *total* absorptivity and *total* transmissivity coefficients averaged inside the *shortwave* radiation band⁹ (α, τ).

Similarly when dealing with thermal radiation we will consider *total* absorptivity and *total* transmissivity coefficients averaged inside the *longwave* radiation band⁹ (α_{IR}, τ_{IR}). In general it is assumed that the longwave absorptivity coefficient α_{IR} is equal to the emissivity coefficient ε ($\alpha_{IR} = \varepsilon$) according to **Kirchhoff's law**^{9,20,29,30}.

As it can be seen in Figure 3.4, the balloon film is not only affected by the outer environment, but also by the inner environment, in particular by the trapping of heat due to *multiple internal reflections*⁹. These multiple reflections raise the effective interior absorption. In order to take into account this effect, an “effective” reflectivity coefficient⁹, r_{eff} , can be defined.

The reflectivity coefficient can be obtained considering the relationship:

$$r = 1 - \alpha - \tau$$

As it is shown in Ref. 9, r_{eff} can be defined as:

$$r_{eff} = r + r^2 + r^3 + r^4 + \dots$$

Considering that:

$$1 + r_{eff} = 1 + r + r^2 + r^3 + r^4 + \dots$$

and taking advantage of the geometric series, this factor can be re-written in terms of the reflectivity coefficient r .

$$1 + r_{eff} = 1 + r + r^2 + r^3 + r^4 + \dots = \frac{1}{1-r}$$

Equally, an $r_{eff_{IR}}$ can be defined for the *longwave* reflectivity coefficient.

In addition, when evaluating the heat loads due to albedo and thermal ground emission it must be considered the effective balloon area exposed to the planet surface. Consequently, a view factor is defined²⁰:

$$ViewFactor = \frac{(1 - \cos(HalfCone_{angle}))}{2}$$

where the half cone angle is:

$$HalfCone_{angle} = \sin^{-1} \left[\frac{R_{Earth}}{R_{Earth} + Z} \right]$$

In fact when $Z = 0$, $HalfCone_{angle} = 90$ deg and $ViewFactor = 0.5$. Therefore at launch, the exposed balloon area is 50% of the surface area. Then it gradually decreases as the balloon rises (for instance, at 30 km of altitude $ViewFactor \cong 0.45$).

3.2.4.2 – Heat Loads

Now it is possible to write the complete set of heat loads acting on the balloon combining the thermal fluxes with the optical properties of the balloon and the exposed surfaces.

- Total absorbed direct sun radiation:

$$Q_{Sun} = \alpha A_{projected} \cdot q_{Sun} [1 + \tau(1 + r_{eff})]$$

that, according to the previous remarks, can be rewritten as:

$$Q_{Sun} = \alpha A_{projected} \cdot q_{Sun} \left[1 + \frac{\tau}{1-r} \right] \quad [\text{W}]$$

- Total absorbed albedo heat:

$$Q_{Albedo} = \alpha A_{surf} \cdot q_{Albedo} ViewFactor \left[1 + \tau(1 + r_{eff}) \right]$$

$$\Downarrow$$

$$Q_{Albedo} = \alpha A_{surf} \cdot q_{Albedo} ViewFactor \left[1 + \frac{\tau}{1-r} \right] \quad [\text{W}]$$

- Total absorbed planetary longwave heat:

$$Q_{IREarth} = \alpha_{IR} A_{surf} \cdot q_{IREarth} ViewFactor \left[1 + \tau_{IR} (1 + r_{eff_{IR}}) \right]$$

$$\Downarrow$$

$$Q_{IREarth} = \alpha_{IR} A_{surf} \cdot q_{IREarth} ViewFactor \left[1 + \frac{\tau_{IR}}{1-r_{IR}} \right] \quad [\text{W}]$$

- Absorbed IR self-glow from the interior:

$$Q_{IRFilm} = \sigma \epsilon \alpha_{IR} A_{surf} T_{film}^4 (1 + r_{eff_{IR}})$$

$$\Downarrow$$

$$Q_{IRFilm} = \sigma \epsilon \alpha_{IR} A_{surf} T_{film}^4 \frac{1}{1-r_{IR}} \quad [\text{W}]$$

- Emitted energy from both the interior and exterior of the balloon skin:

$$Q_{IROut} = \sigma \epsilon A_{surf} T_{film}^4 \left[1 + \tau_{IR} (1 + r_{eff_{IR}}) \right]$$

$$\Downarrow$$

$$Q_{IROut} = \sigma \epsilon A_{surf} T_{film}^4 \left[1 + \frac{\tau_{IR}}{1-r_{IR}} \right] \quad [\text{W}]$$

- External convective heat load:

$$Q_{ConvExt} = HC_{external} A_{effective} (T_{air} - T_{film}) \quad [W]$$

- Internal convective heat load:

$$Q_{ConvInt} = HC_{internal} A_{effective} (T_{film} - T_{gas}) \quad [W]$$

3.2.5 – Heat Transfer Differential Equations

As stated earlier, the vertical motion of balloon systems depends critically on the heat transfer to and from the gas inside⁹, because the temperature and the density of the gas determine the lift of the balloon. It is therefore necessary to take into account the rate of change of temperature of both the gas and the balloon film.

The rate of change of the lifting gas temperature is formulated on the adiabatic expansion response modified with the internal free convection interaction with the film^{9,17,18,20}.

The First Law of thermodynamics for an ideal gas can be formulated in differential form as follows:

$$du = c_v dT = \delta Q - pdV$$

By combining this equation with the ideal gas law, the following differential equation is obtained:

$$\dot{T}_{gas} = \frac{Q_{ConvInt}}{c_v M_{gas}} + (\gamma - 1) \frac{T_{gas}}{\rho_{gas}} \frac{d\rho_{gas}}{dt}$$

This equation does not include the loss of energy due to mass flow (i.e. during valving and/or venting). This effect will be added in future enhancements of this model.

Using the hydrostatic equation and the **zero-pressure** assumption:

$$\frac{dp_{air}}{dh} = -\rho_{air} g \quad p_{air} \approx p_{gas}$$

the previous differential equation can be rewritten as:

$$\dot{T}_{gas} = \frac{Q_{ConvInt}}{\gamma c_v M_{gas}} - \frac{(\gamma-1)}{\gamma} \frac{\rho_{air} g}{\rho_{gas} R_{gas}} \cdot RoC$$

where RoC is the rate of climb ($RoC = -V_z$).

The rate of change of the film temperature is derived from the simple transient energy-balance equation. The “minus” sign indicates heat loss.

$$\dot{T}_{film} = \frac{(Q_{Sun} + Q_{Albedo} + Q_{IREarth} + Q_{IRfilm} + Q_{ConvExt} - Q_{ConvInt} - Q_{IRout})}{c_f M_{film}}$$

3.2.6 – Valve and Duct Flow Differential Equations

As previously stated, zero-pressure balloons have large open ducts at the base of the envelope in order to vent the excess gas so that the pressure differential from inside and to outside remains small. Gas expulsion occurs whenever the balloon is at its maximum volume and continues to ascend due to inertia or momentum^{8,17}. Since a zero-pressure balloon is always launched with excess free lift (excess gas), these phenomena almost always occur as the balloon goes into float.

In addition since in many flights operational specifications may require a decrease in altitude or an increase of the descent velocity, balloons present valves at the top of the envelope that allow a certain degree of altitude control^{8,20}.

Flow through a duct or a valve depends on the differential pressure across the area interface, on the cross sectional area, on the density of gas and on a discharge coefficient^{8,9,20}.

The mass rate of change due to venting and valving is modeled with the following equation:

$$\dot{M}_{gas} = -\left(A_{duct} C'_{discharge} \sqrt{2\Delta P_{duct} \rho_{gas}} + A_{valve} C''_{discharge} \sqrt{2\Delta P_{valve} \rho_{gas}}\right)$$

This equation essentially derives from Bernoulli's Equation. $C'_{discharge}$ and $C''_{discharge}$ are discharge coefficients that account for all deviations of the actual flow from the theoretical flow⁹. The discharge coefficient cannot exceed 1 and it is rarely below 0.5.

The differential pressure ΔP can be evaluated as follows.

The pressure difference can be assessed considering the hydrostatic equation⁹:

$$p_{gas} - p_{air} = g(\rho_{air} - \rho_{gas})h$$

where h is the vertical distance from the zero-pressure level to the opening (duct or valve). Since at the float altitude the zero-pressure level is usually at the bottom of the balloon, h is the distance between the bottom of the balloon and the opening.

Valves are usually located at the top of the balloon, therefore in this case h will be equal to the height of the balloon. According to the geometric properties defined in the previous paragraphs:

$$h_{valve} = Height = 0.748 \cdot Diameter = 0.748 \cdot 1.383 \cdot Volume^{\frac{1}{3}} = 1.034 \cdot Volume^{\frac{1}{3}}$$

Therefore the pressure difference across the valve:

$$\Delta P_{valve} = g(\rho_{air} - \rho_{gas}) \cdot 1.034 \cdot Volume^{\frac{1}{3}}$$

In zero-pressure balloons, *Venting Ducts Length* can be found on the datasheet. This *Length* can be expressed as a fraction of the total balloon *Height* (at maximum volume).

For instance if:

$$Height = 69.75 \text{ m} \quad (\text{from datasheet})$$

$$Length = 33 \text{ m} \quad (\text{from datasheet})$$

the ducts are located at approximately $\frac{Length}{Height} = 47\%$ of the total height of the balloon.

Therefore,

$$h_{duct} = 0.47h_{valve}$$

So finally the pressure difference across the duct is:

$$\Delta P_{duct} = g(\rho_{air} - \rho_{gas}) \cdot h_{duct} \quad [\text{Pa}]$$

3.2.7 – Ballasting

As for valving, a balloon may need ballast drop due to environmental conditions and/or operational requirements (i.e. to increase the rate of climb). In the present model ballasting is handled straightforwardly.

Given a **ballast discharge rate** k_{ball} , the gross mass (M_{gross}) is reduced for *each* ballast drop according to the following equation:

$$M_{gross} = M_{gross\ actual} - \int_{\Delta t} k_{ball} dt \quad [\text{kg}]$$

where $M_{gross\ actual}$ is the actual gross mass before ballasting, and Δt is the discharge time interval. Of course at launch $M_{gross\ actual}$ is equal to the initial gross mass.

3.2.8 – Closing Remarks

Of course, in order to close the model, the balloon *Volume* must be evaluated. This can be done using the perfect gas law and considering the zero-pressure assumption. Actually, knowing altitude (and hence air pressure), gas temperature and gas mass:

$$p_{air} \approx p_{gas} \quad Volume = M_{gas} R_{gas} \frac{T_{gas}}{p_{gas}}$$

4

ACHAB at Work

The purpose of this chapter is to present the main features, the inputs and the outputs of ACHAB, the balloon flight simulation code described in the previous chapter. This general overview will be done by setting up and running an illustrative simulation.

4.1 – ACHAB Simulation Environment

The balloon theoretical model presented in the previous chapter was implemented in a computer simulation tool developed in Matlab/Simulink environment. This tool allows to analyze the performance of the balloon flight predicting 3D position and velocity along with balloon film temperature and lifting gas temperature and volume. The simulation code can also handle gas valving and ballasting, allowing the characterization of different altitude control strategies.

The details of the simulation tool (reference version: ACHAB v1.0) will be explained assuming a standard zero-pressure balloon whose characteristics will be specified in the following sections.

4.2 – Input Data

The simulation tool needs several input and initial data in order to assess the balloon performance. As a reference for them, it is here considered a nominal USV-DTFT1 mission (see Chapter 2) including the characteristics of the balloon chosen for the mission.

When the necessary data are not available from applicable documents, *typical* zero-pressure scientific balloon characteristics, as identifiable from references, are considered in the simulation.

In the present version, a Matlab script handles the input of the initial data and the computation of several derived quantities.

The required data are grouped in the following categories.

4.2.1 – Balloon Characteristics

The most important balloon characteristics that have to be specified as input data are:

- balloon mass and volume properties (including payload and ballast mass)
- aerodynamic drag coefficient (if considered constant)
- film radiative properties
- geometric characteristics of valves and venting ducts.

Most of these properties mentioned above are specified by the balloon (or film) manufacturer and must be taken from the *datasheet*.

4.2.1.1 – Mass and Volume Properties

First of all, the **payload mass** must be specified in order to choose the size of the balloon volume and/or the float altitude. To this end, manufacturers may provide

gross load vs. theoretical float altitude curves (based on standard atmosphere) parameterized with the design volume of the balloon. The gross load includes the balloon mass.

According to our available data (**datasheet**) the balloon has a *maximum design volume* of:

$$Volume_{Design} = 334705 \text{ m}^3$$

and, according to the manufacturer, a mass of:

$$M_{film} = 1433 \text{ kg}$$

and must lift a payload mass of:

$$M_{load} + M_{ballast} = 3054 \text{ kg}$$

This quantity is considered as the sum of the following masses: USV vehicle, Gondola, flight chain. See Table for details.

Mass Budget	[kg]
Gondola (Avionics – No Ballast)	837
Ballast	500
Flight Chain	325
Other masses	71
USV - Vehicle	1321
Total	3054

Table 4.1 – Mass Budget for the DTFT1 mission payload.

Therefore the gross mass of the system is:

$$M_{gross} = M_{film} + M_{load} + M_{ballast} = 4487 \text{ kg}$$

In addition, as stated in the previous chapter, as the balloon rises, the *added mass* effect must be taken into account when the balloon rises. According to Ref. 20, the added mass coefficient considered is a mean value:

$$C_{added} \approx 0.37$$

Another important balloon characteristic is the maximum diameter. This value is reported on the datasheet.

$$MaxDiameter = 96.80 \text{ m}$$

The initialization script calculates automatically the design *gore length* according to the equation reported in Chapter 3.

4.2.1.2 – Geometric Characteristics of Venting Ducts and Valves

The geometric properties of the gas venting ducts and valves are essentially the areas of the openings (from datasheet) and the discharge coefficient, both necessary for the computation of the mass flow:

$$A_{duct} = 11.6 \text{ m}^2 \quad C'_{discharge} = 0.62 \quad nDucts = 3 \text{ (number of ducts)}$$

The balloon has 3 valves at the top. The diameter of each valve is 0.35 m and therefore:

$$A_{valve} = \pi \left(\frac{0.35}{2} \right)^2 = 0.096 \text{ m}^2 \quad C''_{discharge} = 0.82 \quad nValves = 3$$

It is worth noting that the $C''_{discharge}$ coefficient is equal to 1 when the valving process starts and decreases to the reported value once the valves are completely opened.

In the present version of the software it is possible to enable or disable valving according to the simulation purposes by specifying a Boolean variable (1, On – 0, Off).

It is also necessary to specify:

- the time instant (in seconds) from balloon lift off in which valves have to be opened. For example:

$$\text{ValveTime} = 8000 \text{ [s]}$$

- the time interval (in seconds) between the starting and the ending of valves' opening process:

$$T_{on} = 20 \text{ [s]}$$

- the time interval (in seconds) between the starting and the ending of valves' closing process:

$$T_{off} = 20 \text{ [s]}$$

- the time interval (in seconds) between the end of valves' opening process and the start of valves' closing process. For example:

$$\text{CloseTime} = 2000 \text{ [s]}$$

The valves can only be opened **all** at the same time. A sequential valves' opening and closing process, compliant to the balloon flight operations, has been studied, but it does not seem to improve the model performances.

The present valving model is still in development. Future versions of ACHAB will provide a better valving model.

4.2.1.3 – Film Radiative Properties

Film radiative properties are vital to the correct prediction of the balloon flight performance. Yet the exact knowledge of these properties can be very challenging. Due to the large variety of film types and of film coatings, thermal radiative properties can be completely different for different balloons, giving distinct ascent characteristics to balloons.

As an example of this variety, Table (Ref. 9) shows radiative properties of several different balloon coatings.

Material	IR Emissivity, ε	Solar Absorption, α	Ratio, α/ε
Silver (polished)	0.02	0.07	3.50
Platinum	0.05	0.10	2.00
Aluminum	0.08	0.15	1.88
Nickel	0.12	0.15	1.25
Aluminum paint	0.55	0.55	1.00
White lead paint	0.95	0.25	0.26
Zinc oxide paint	0.95	0.30	0.32
Gray paint	0.95	0.75	0.79
Black paint	0.95	0.95	1.00
Lamp black	0.95	0.97	1.02
Silver sulfide	0.03	0.60	20.00
Nickel black	0.10	0.90	9.00
Cupric oxide	0.15	0.90	6.00

Table 4.2 – Radiative properties of several different balloon coatings (Ref. 9).

Typically, balloons are made of **Polyethylene**.

According to data supplied by the balloon manufacturer, the specific heat of the polyethylene film is:

$$c_f = 2092 \text{ J/kg/K}$$

and the thermal radiative properties of the balloon film (as specified in Chapter 3) are the following:

$$\begin{aligned} \alpha &= 0.024 & \tau &= 0.916 \\ \alpha_{IR} &= 0.1 & \tau_{IR} &= 0.86 \end{aligned}$$

Of course, $r = 1 - \alpha - \tau$ and $r_{IR} = 1 - \alpha_{IR} - \tau_{IR}$.

4.2.1.4 – Aerodynamic Drag Coefficient

As stated in the previous chapter, in this model it is possible to choose either to use a variable drag coefficient (as suggested by the present author²⁶) or a constant drag coefficient.

Since several past studies^{18,19} have proved that good correlation with flight data can be obtained in certain conditions with a constant aerodynamic drag coefficient (**but - of course - using a different simulation program**), the user can force ACHAB to use a constant and customizable C_d rather than a variable C_d . This can be specified via a Boolean variable,

$$ConstantDragCoeff = \begin{cases} 0 & \text{Not Constant} \\ 1 & \text{Constant} \end{cases}$$

4.2.2 – Location, Date and Time of Launch

In order to correctly simulate the thermal environment and the balloon trajectory, the user must specify launch base location coordinates and the date and time of launch. For instance, USV-DTFT1 launch base location is Arbatax-Tortoli Airport, Italy:

$$LaunchBaseLocation = \begin{cases} lat : & 39.9161^\circ \\ long : & 9.6889^\circ \\ alt : & 0 \text{ m} \end{cases}$$

Let's suppose a flight on January, 16 2006 at 08:00:00, local time:

$$DateOfLaunch = 16-01-2006 08:00:00$$

The code needs information on *daylight saving* and *time zone*. Daylight saving is a Boolean variable, while the time zone is the number of hours (positive or negative) with respect to Greenwich.

In this example:

$$DaylightSaving = 0$$

$$Timezone = +1 \quad (\text{i.e. 1 hour east of Greenwich})$$

4.2.3 – Ballasting

ACHAB manages ballasting using a Ballast Discharge List, which is a list of the scheduled ballast drops as a function of the elapsed time from lift-off (in seconds).

$$BallastDischargeList = [TimeFromLiftOff \quad Ballast]$$

Currently ACHAB supports a maximum of 30 ballast drops.

For example, if the user wants to command 2 ballast drops of 150 kg and 350 kg after 5000 seconds and 13000 of flight respectively, the Ballast Discharge List will be:

$$BallastDischargeList = \begin{bmatrix} 0 & 0 \\ \vdots & \vdots \\ 0 & 0 \\ 5000 & 150 \\ 13000 & 350 \end{bmatrix}$$

Of course the user must specify the **ballast discharge rate** k_{ball} (in kg/min), usually determined experimentally before the flight from the ballast discharge device.

For example:

$$k_{ball} = 13.1 \quad [\text{kg/min}]$$

4.2.4 – Thermodynamic Data

The thermodynamic data are basically the characteristics of the lifting gas (Helium) and air:

- The **gas constants**:

$$R_{gas} = 2077.25 \text{ J/kg/K} \quad \text{for helium}$$

$$R_{air} = 287.05 \text{ J/kg/K} \quad \text{for air}$$

- Specific heat at constant volume for helium:

$$c_v = 3115.89 \text{ J/kg/K}$$

- and the specific heat ratio (for helium):

$$\gamma = 1.667$$

The user can also specify a different value for the nominal (mean) solar constant:

$$I_{Sun0} = 1367.7 \quad [\text{W/m}^2]$$

4.2.5 – Atmospheric Data

The user must input to ACHAB a *three-dimensional atmospheric model*. This means that:

- air pressure [Pa]
- air temperature [K]
- north wind component [m/s]
- east wind component [m/s]

are a function of latitude, longitude and altitude.

Actually these data must be defined inside a 3D grid that contains the area in which the flight should take place. For example:

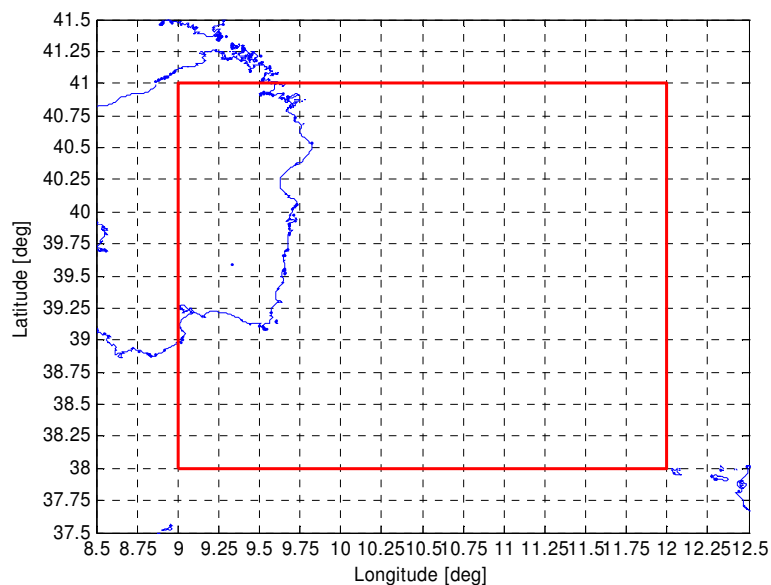


Figure 4.1 – Atmospheric data area.

Figure 4.1 shows (in red) the borders of the area in which atmospheric data are available for the simulation.

These data – that can be provided by any weather forecast service – are loaded inside the model using look-up tables that interpolate between longitudes, latitudes and altitudes. For our simulations we have used the **ECMWF** atmospheric data⁴¹.

4.2.6 – Albedo Factor

Another important atmospheric parameter is the *Albedo* factor which is fundamental for the computation of one of the thermal loads acting on the balloon.

As stated in the previous chapter the present model considers a constant albedo factor throughout the entire flight.

Future releases of ACHAB will take into account albedo variations due to the nature of the Earth's surface properties over which the flight takes place^{34,35}.

For balloon flights over sea surfaces it has been considered a mean albedo factor of:

$$Albedo = 0.10$$

It is known that the albedo factor over the sea surface can vary remarkably especially with latitude and sun angle. According Ref. 33, *Albedo* = 0.10 is a good mean value for water at latitudes around 40°N during winter (the launch site considered in this example is Arbatax, Italy).

4.2.7 – Initial Data

Finally, initial data must be specified to allow the integration of the equations. The initial position and velocity are given in NED reference frame:

$$x_0 = 0 \quad y_0 = 0 \quad z_0 = 0$$

$$V_N = 0 \quad V_E = 0 \quad V_D = 0$$

As to the thermodynamic data:

- ground atmospheric temperature T_{0air} : it is provided by the atmosphere model
- ground atmospheric pressure p_{0air} : it is provided by the atmosphere model
- ground gas temperature T_{0gas} : it is assumed equal to T_{0air}
- ground gas pressure p_{0gas} : it is equal to p_{0air} because of the zero-pressure assumption.

4.2.8 – Initial Gas Mass and Free Lift

According to the user's requirements, it is possible to either specify the initial lifting **gas mass** or the desired amount of **nominal free lift**.

When inflating a large scientific balloon it is often difficult to accurately determine the amount of lifting gas loaded inside the envelope⁹. This is due to the fact that the thermodynamic process that regulates the mass flow between the helium tanks and the balloon film is difficult to model⁹. The exact amount can be usually determined only long after lift-off, when helium tanks have regained thermodynamic equilibrium. Therefore, when using ACHAB, this source of **uncertainty** must be taken into account.

Typical values of the nominal free lift are around 10% - 20%. It must be kept in mind that choosing too large a value of free lift may produce high vertical speeds that might result in excessive cooling of the balloon film which could ultimately reach the *glass transition temperature* and burst^{17,36,37}.

ACHAB is capable of checking if the polyethylene cold-brittle point is reached by monitoring the T_{film} variable (see Figure 4.4).

If the Boolean variable USE_FL (use free lift) is 0 then the user must input the value of the initial mass, M_{gas0} .

Alternatively if USE_FL is 1, then the user must specify the desired amount of free lift (in percentage). Consequently the code determines the mass of gas (helium) according to the following formula (**definition of nominal free-lift**) (Ref. 9):

$$M_{gas0} = \frac{M_{gross} \left(\frac{FreeLift}{100} + 1 \right)}{\frac{MW_{air}}{MW_{gas}} - 1} \quad [\text{kg}]$$

where *FreeLift* is the percentage free lift and MW_{air} and MW_{gas} are the molecular weights of air and lifting gas (helium).

For example, using the mass data defined in the previous paragraphs and choosing a

$$FreeLift = 11\%$$

we will have:

$$M_{gas0} = 798.63 \text{ [kg]}$$

4.3 – Illustrative Simulation: Results

In this section the outputs of an illustrative simulation carried out by ACHAB will be presented. Inputs to the simulator are those specified in the previous paragraphs.

Figure 4.2 shows the ascent profile of the balloon. After 10 minutes since the attainment of the float altitude, valves are opened and the balloon starts to descend until it reaches a descent velocity of 4 m/s (Figure 4.3) when valves are closed.

Figure 4.4 shows the temperature profiles of both the helium and the balloon film. It can be seen that the film temperature does not go below 193K (~ -80°C) which is the ***cold-brittle point*** for polyethylene (Ref. 17). The attainment of that temperature (due to an excessive ascent velocity) could actually cause a catastrophic loss of the balloon.

Figure 4.5 shows the gas mass flow rate while Figure 4.6 shows the balloon volume profile. It can be seen that at float altitude the balloon has actually reached its design volume. Figure 4.7 shows the ballast drop profile.

Finally, Figure 4.8 shows a 3D plot of the balloon trajectory above the Balloon Launch Base in Arbatax (Sardinia, Italy).

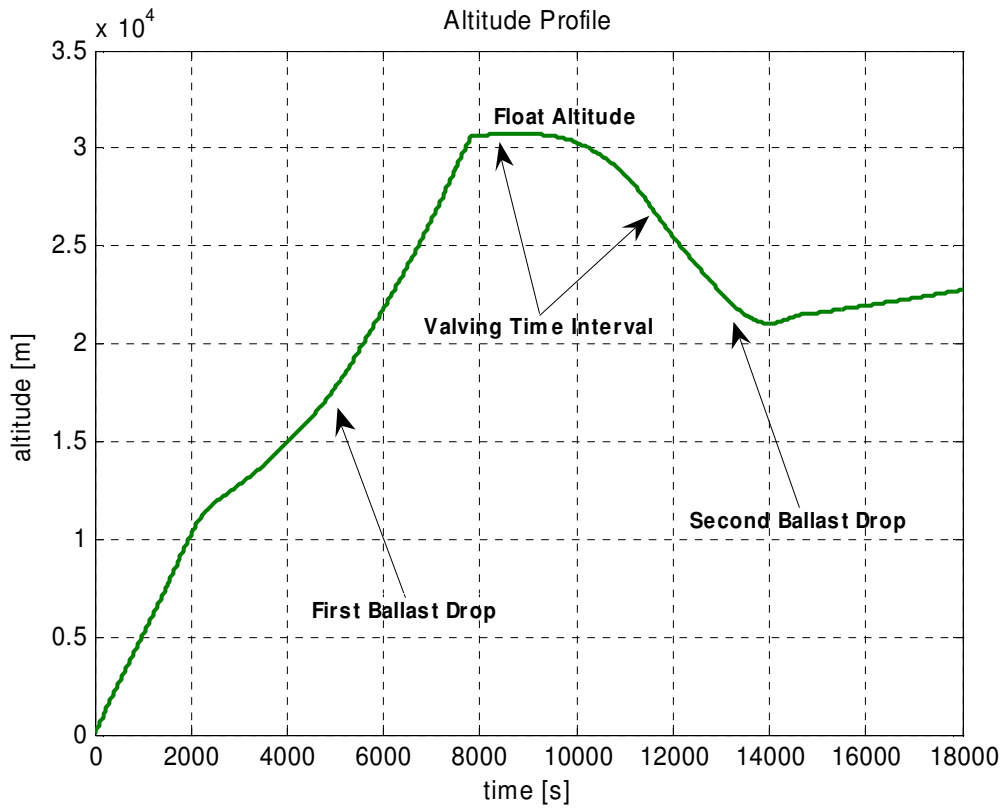


Figure 4.2 – Ascent Profile.

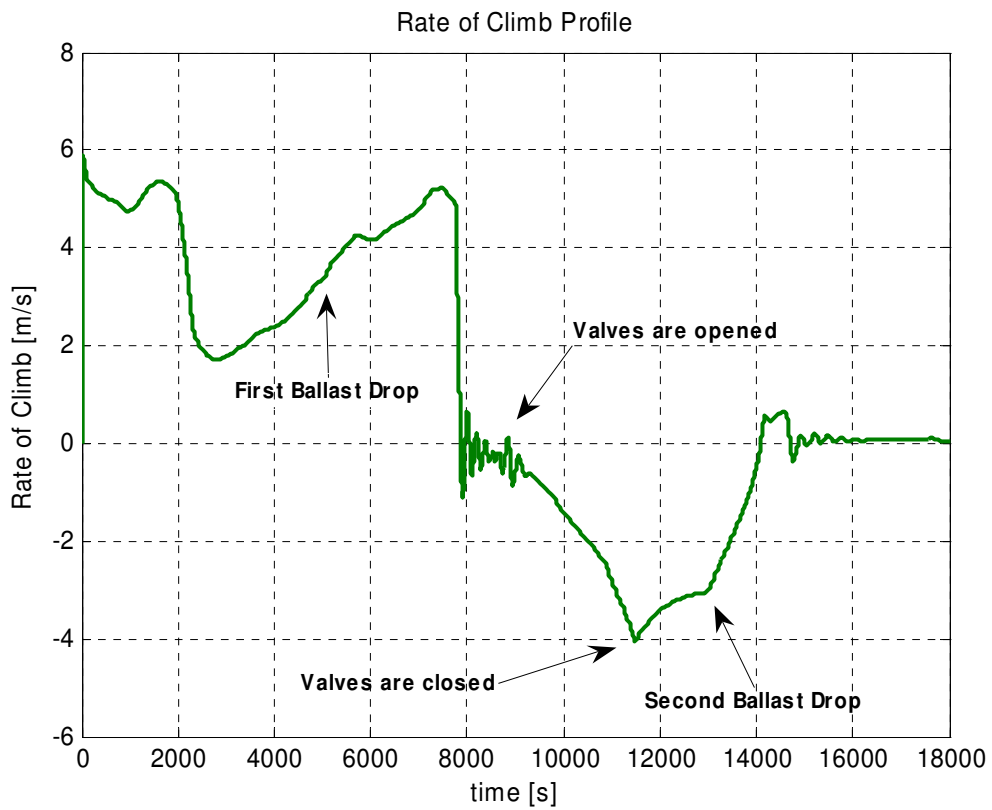


Figure 4.3 – Rate of Climb.

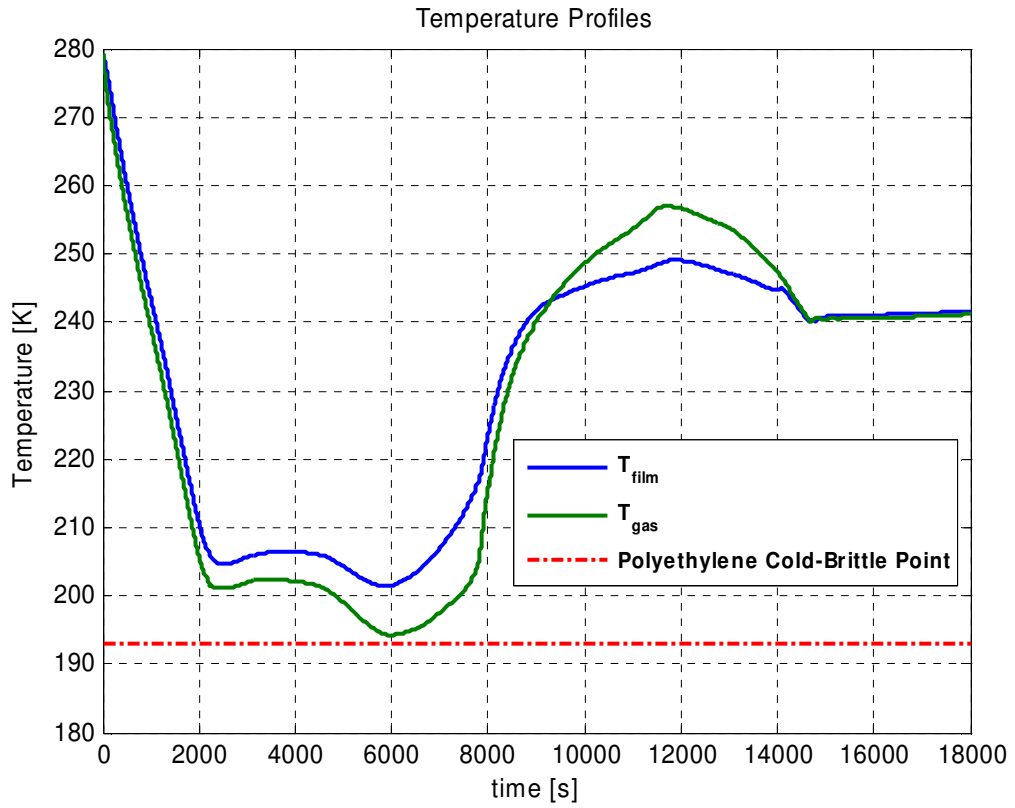


Figure 4.4 – Gas and Film Temperature.

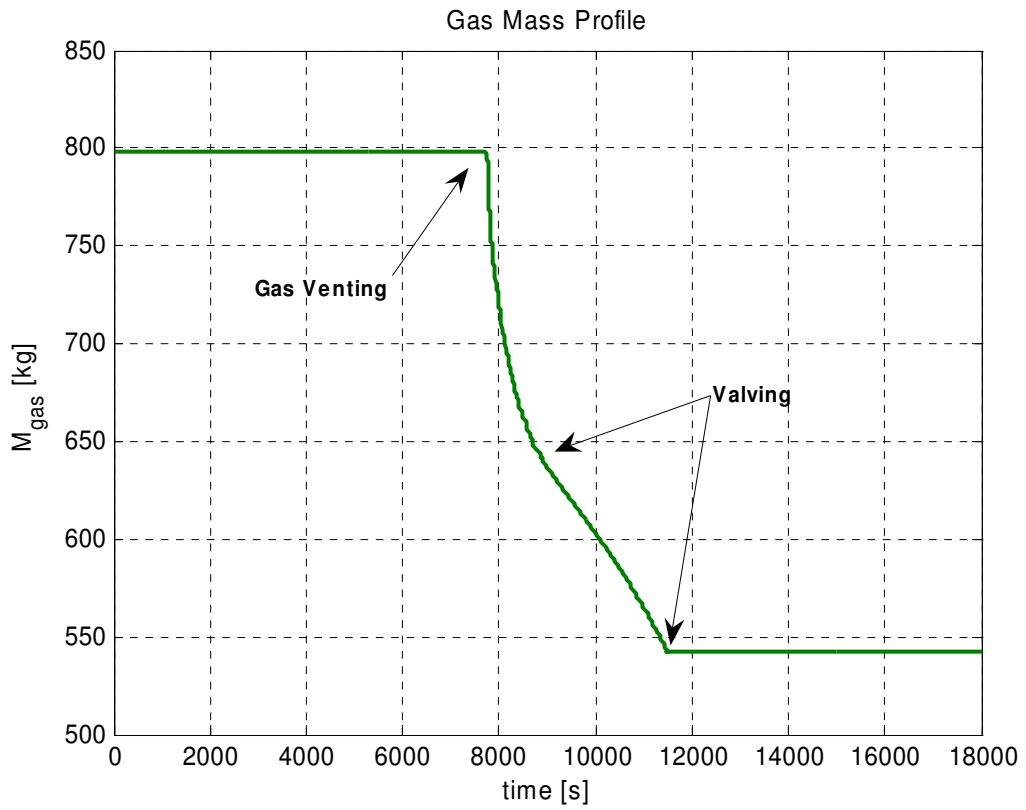


Figure 4.5 – Gas Mass profile.

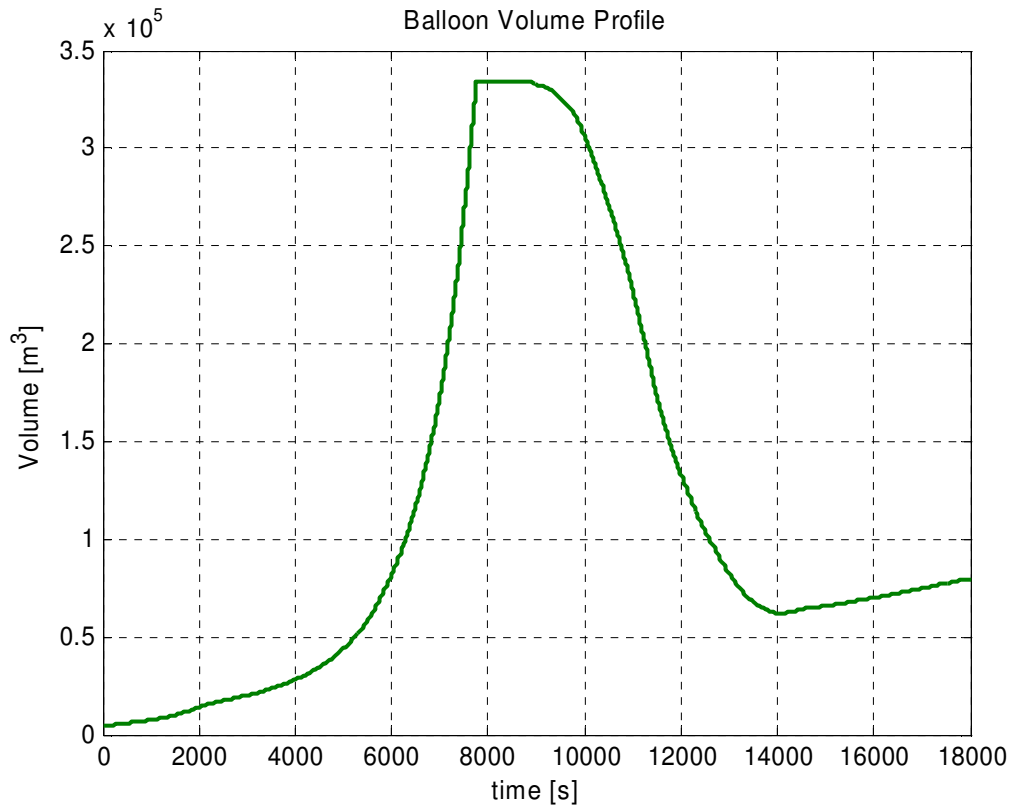


Figure 4.6 – Balloon Volume.

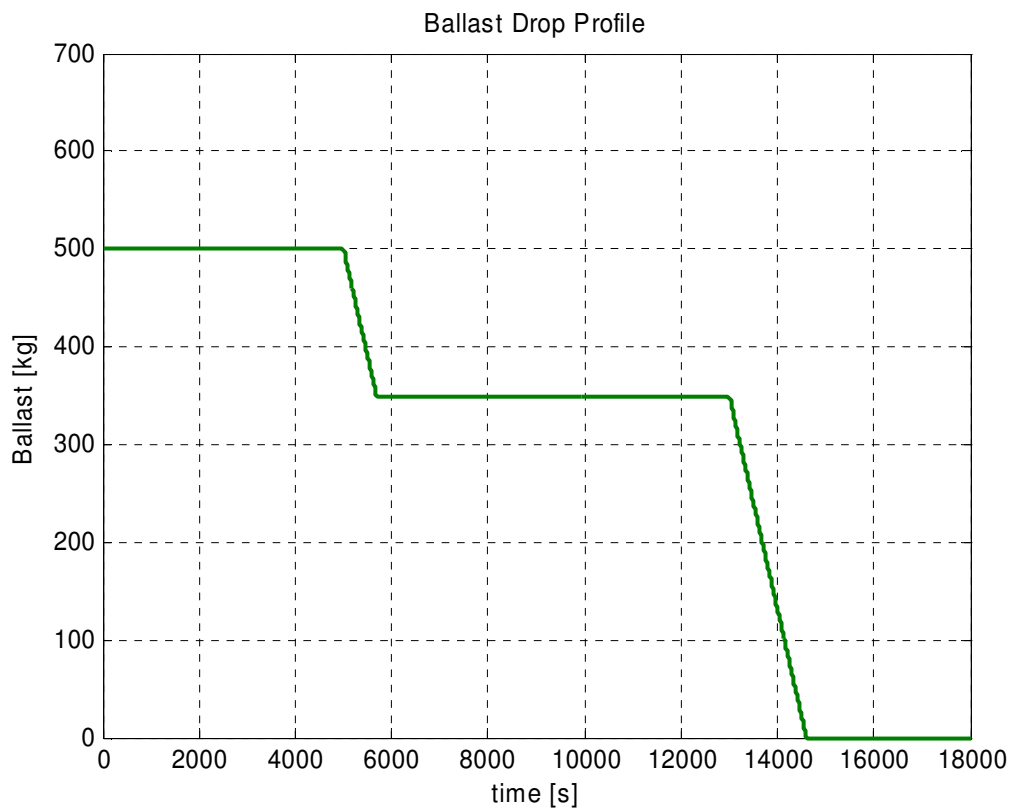


Figure 4.7 – Ballast Drop Profile.

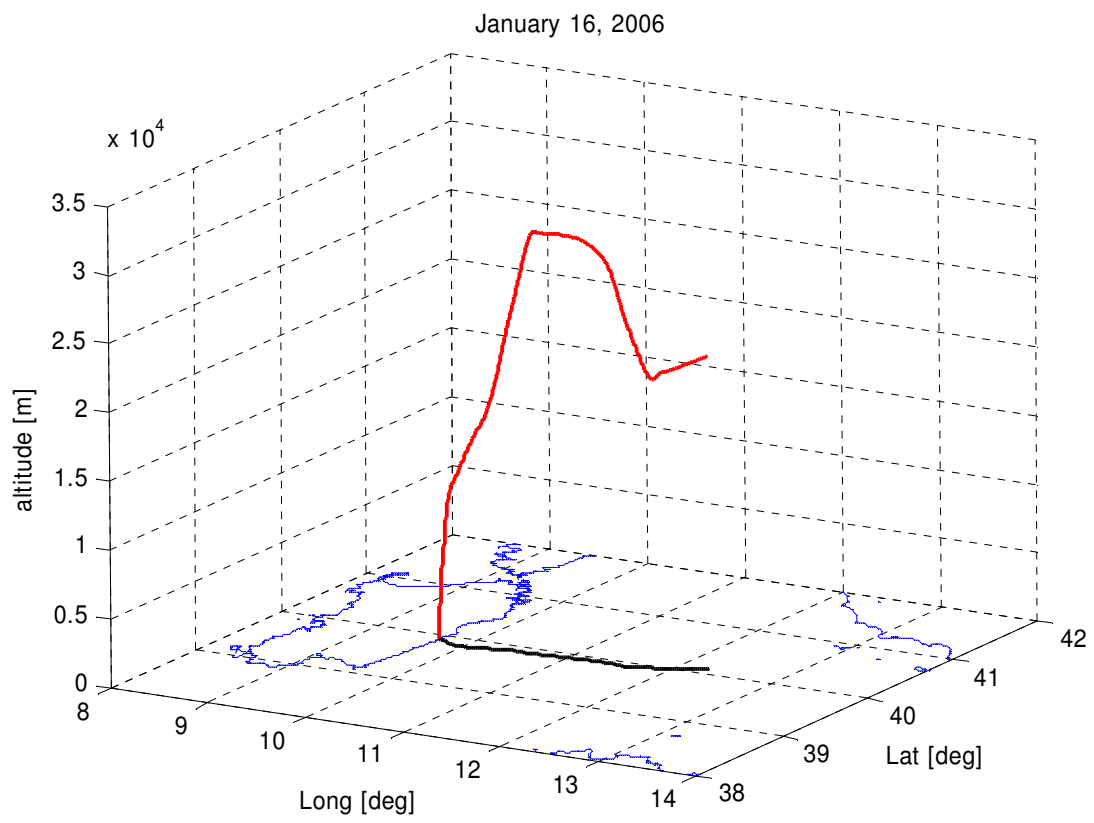


Figure 4.8 – 3D view of the balloon trajectory.

5

Validation of the Code

The purpose of this chapter is to present the validation process of ACHAB. The performance of the code was evaluated comparing the simulation results to some available real balloon flight data.

5.1 – Validation Procedure

ACHAB has been validated comparing simulation results with GPS recorded data of different balloon flights. At the time of writing, only a restricted number of data are available for validation purposes.

The flight data, balloon details, weather data, atmospheric information and surface characteristics were obtained from Ref. 7, 26, 34, 35, 39, 40, 41, 43, 44, 49, 50.

During validation tests, ACHAB was also compared to the outputs of NASA's Scientific Balloon Analysis Model (SINBAD v3.1G).

5.1.1 – A note about SINBAD

It is far beyond the scope of this work to give an overview of SINBAD and of its performance (some insight on this subject may be given by Ref. 19 and Ref. 38). However it is certainly possible to remark some evident differences between SINBAD and ACHAB, which have been identified from the simulation results and SINBAD user manual (SINBAD source code was *not available*).

- SINBAD uses a 5-point one-dimensional atmospheric model. More precisely, the user can specify 5 air temperature points (temperature vs. altitude) or choose between different built-in atmospheric models. Air pressure can be provided only at launch site altitude. Conversely, ACHAB can use a detailed atmospheric model which can also be the meteorological forecast model data of the launch area.
- SINBAD uses a constant drag coefficient, while ACHAB uses a profiled drag coefficient to take into account the effects of the transition through troposphere.
- SINBAD does not support horizontal winds, while ACHAB does.
- SINBAD computes only the vertical motion of the balloon. No trajectory visualization/tracking can be done.
- In SINBAD the user must input a 5 point black-ball temperature profile in order to take into account IR environment effects; in ACHAB the user must specify a ground temperature and a ground emissivity coefficient.

In addition, the definition of some input parameters in both codes is not the same. Therefore some time has been spent in order to derive correct conversion rules to ensure the use of same simulation inputs to both models as much as possible with the purpose of making valid comparisons.

In summary, the differences listed above between SINBAD and ACHAB, together with possible and unknown modeling differences, might explain the discrepancies in simulation results between the two tools.

5.2 – Case 1 – HASI 2003 Balloon Flight

HASI 2003 (Huygens Atmospheric Structure Instrument) was a balloon flight mission that had as objective the simulation of the Huygens probe mission on Titan in the terrestrial atmosphere⁴⁰.

5.2.1 – Advantages and Limitations of the Available Flight Data

Data provided for Case 1 had several advantages. We had at our disposal:

1. the original balloon datasheet
2. weighing table (completed just before launch)
3. location, date and time of launch
4. wind and atmosphere sounding
5. digital GPS data (position and velocity)
6. error evaluation on the initial gas mass (lifting force) (i.e. accurate knowledge of the initial gas mass).

On the other hand, there were also some limitations:

1. no precise measurement of air temperature and air pressure at launch
2. one-dimensional atmospheric data
3. no ballast release history
4. no accurate information on the optical-radiative properties of the balloon film in use

Nonetheless, the HASI 2003 balloon flight appeared to us as a sufficiently complete data set suitable to provide a preliminary outlook on the validity of the code and on its performance.

5.2.2 – Input Data

Main characteristics of the system (which have been used for simulations with both tools):

- **Balloon Volume:** 98862 m³
- **Payload Mass:** 457.5 kg (no ballast)
- **Ballast:** 150 kg
- **Percentage Free Lift:** 12%
- **Error evaluation on the loaded lift force (gas mass):** << 0.5%
- **Atmospheric sounding of the day of launch** (data were adapted to suit each simulation tool)
- **Ballast Release History:** N/A
- **Location, Date and Time of Launch:** Trapani-Milo Launch Base – Jun. 07, 2003 – 04:54 UTC (06:54 local time)
- **Thermo-optical properties of the balloon film:** data provided by the manufacturer for the USV-FTB1 balloon, assuming that the balloon film is essentially the same.

5.2.3 – Results

Figure 5.1 and Figure 5.2 show the rate-of-climb GPS data and the altitude GPS data compared to simulation outputs. It can be seen that ACHAB results are in very good agreement with flight data especially from lift-off to the tropopause.

Since no ballasting information was provided it is not possible to say if there were any significant ballast drops during the ascent phase. Only at float altitude, that rapid change in altitude (evidenced in Figure 5.2) could be explained by a probable ballast drop (which was not simulated because unknown).

On the same figures there are 2 other simulations. The red line is SINBAD output with a drag coefficient of $C_d = 0.45$ (spherical assumption^{39,40}). In this case, SINBAD yields a very similar initial velocity but overestimates the up velocity for subsequent time instants, producing a consistent discrepancy with the GPS altitude profile.

In order to make a comparison with SINBAD, ACHAB was run using the same constant drag coefficient $C_d = 0.45$ (green line). The rate of climb is well approximated almost up to the tropopause. Afterwards the up velocity is overestimated. This behavior is consistent with what observed in Ref. 24 for which changes in the “*dynamical and mechanical responses of the balloon envelope material*” occurring at the tropopause (with consequent structural and shape variations) suggest “*that flight data above and below the tropopause be segregated for the purpose of drag coefficient modeling*”. Therefore, the assumption of a variable drag coefficient appears adequate.

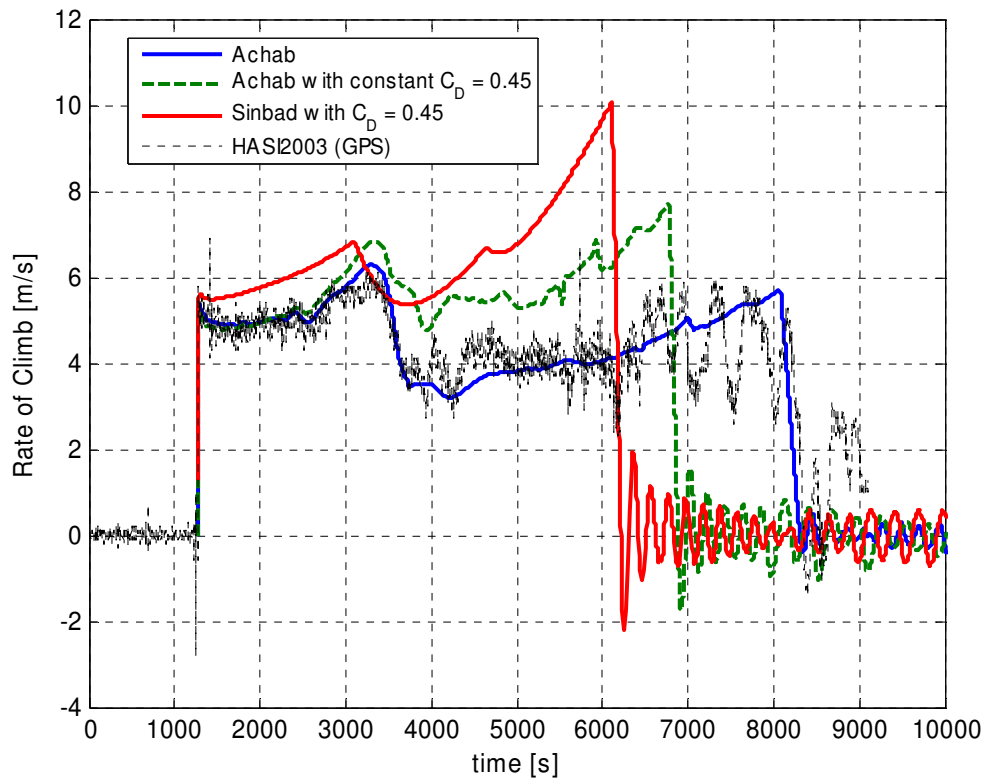


Figure 5.1 – HASI2003 GPS rate of climb data compared to simulation outputs.

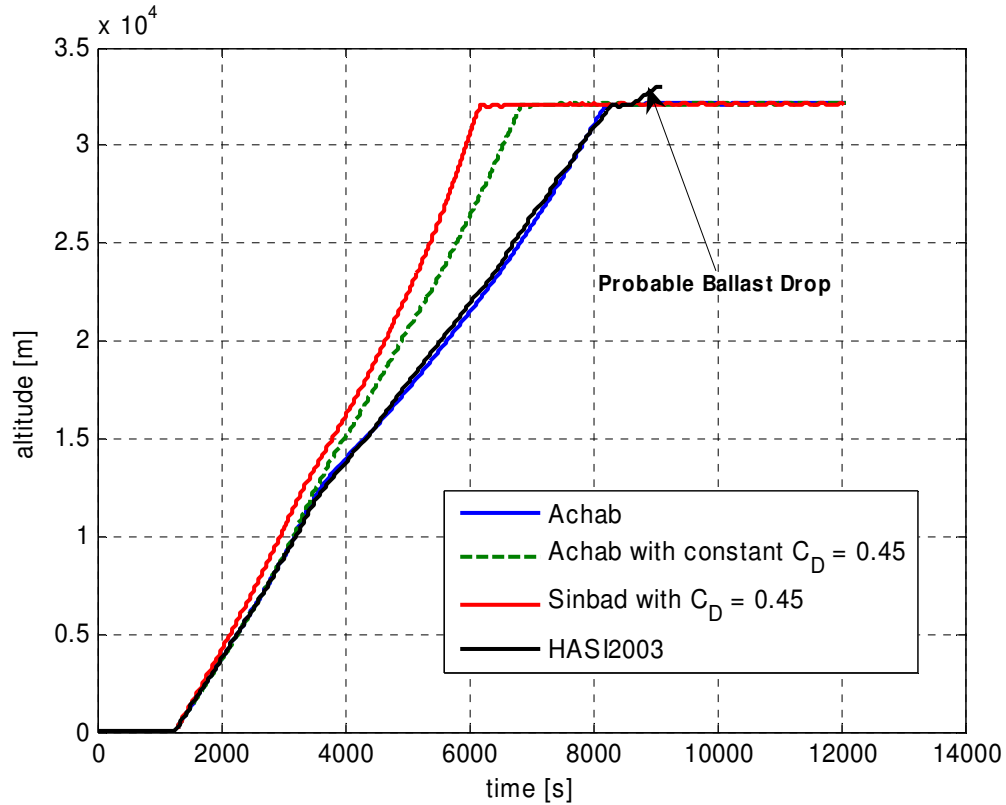


Figure 5.2 - HASI2003 GPS altitude data compared to simulation outputs.

The performance of both simulations (ACHAB and SINBAD) can be evaluated in terms of:

- an *integral error* on the **rate of climb** defined as:

$$\bar{e} = \frac{1}{\Delta T} \int_{t_1}^{t_2} e(t) dt \quad \text{where } e(t) = RoC_{SIMULATED}(t) - RoC_{GPS}(t)$$

- the *root-mean-square (rms) error* on the **rate of climb**.

As stated previously and in Ref. 24, it is reasonable to divide the ascent portion of the flight into a tropospheric phase and a stratospheric phase considering an altitude of about 11500 m as the tropopause altitude. Comparisons between the actual data and the simulations can be done inside these segments.

Table 5.1 reports the comparison between the performance indices introduced earlier evaluated for both simulation programs in the two flight segments and for the global flight (from lift-off up to the float altitude of the real case).

Error [m/s]	Simulator	Tropospheric Flight Segment	Stratospheric Flight Segment	Global Flight
\bar{e}	ACHAB	0.14	0.08	0.10
	SINBAD	0.87	-0.13	0.18
rms	ACHAB	0.28	1.14	0.56
	SINBAD	0.93	5.60	2.70

Table 5.1 – Comparison of the performance indices for the two codes.

The rms error for SINBAD is much higher because its simulation attains the float altitude long before the real flight. This is not evidenced by the integral error because, as it can be seen from Figure 5.1, the large discrepancy between SINBAD and the GPS rate of climb in the stratospheric segment is *on average* small.

Moreover neither of the codes considers the possible oscillations of the balloon that can take place in the stratospheric portion of the flight⁴².

Moreover, according to Ref. 9, in steady conditions (i.e. upward acceleration is zero) it is possible to estimate the initial steady state velocity. This formula does not take into account wind effects:

$$V_{ssZ} = \left| \frac{-2gM_{gross} \left[1 + \frac{M_{gas}}{M_{gross}} \left(1 - \frac{MW_{air}}{MW_{gas}} \right) \right]}{C_d \rho_{air} A_{top}} \right|^{\frac{1}{2}}$$

This is valid when $T_{gas} = T_{air}$ and the upward acceleration is zero.

Using the available data with a $C_d = 0.45$, this formula yields an initial steady velocity:

$$V_{ssZ} \cong 5.3 \text{ [m/s]}$$

which is apparently in good agreement with ACHAB results (Figure 5.3).

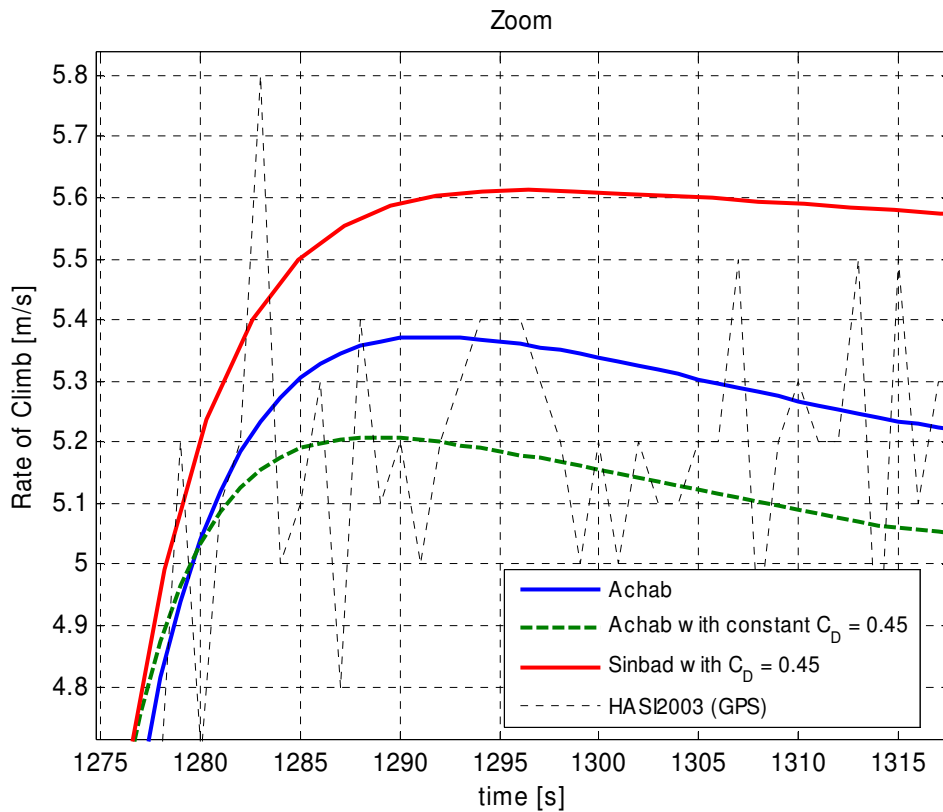


Figure 5.3 – Initial rate of climb.

5.3 – Case 2 – ARD 1995 Balloon Flight Test

The scope of ARD balloon flight test was to qualify the descent and recovery subsystem of the Atmospheric Reentry Demonstrator capsule (ARD). Details can be found on Ref. 43.

5.3.1 – Advantages and Limitations of the Available Flight Data

Data provided for Case 2 were less accurate and more difficult to process. We had at our disposal:

1. weighing table (completed just before launch)
2. location, date and time of launch
3. wind and atmosphere (to be extracted from a table)
4. position and velocity (**to be extracted from a printed plot**)
5. ballast release history

On the other hand, there were also several major limitations:

1. all of the data were on printed paper (**no digital data were available**)
2. no precise measurement of air temperature and air pressure at launch
3. one-dimensional atmospheric data
4. no error evaluation on the loaded gas mass (i.e. **unknown exact gas mass at launch**)
5. most of the quantities had to be **extracted from printed plots**
6. no accurate information on the optical-radiative properties of the balloon film in use

Case 2 has been more difficult to use for validation purposes due to the less accurate data at our disposal. This might in some way account for the discrepancies between the simulation results and the actual flight data.

5.3.2 – Input Data

Main characteristics of the system (which have been used for simulations with both tools):

- **Balloon Volume:** 95339 m³
- **Payload Mass:** 3286 kg (no ballast)
- **Ballast:** 200 kg
- **Percentage Free Lift:** 10%
- **Error evaluation on the loaded lift force (gas mass):** N/A
- **Atmospheric sounding of the day of launch** (data were adapted to suit each simulation tool)
- **Ballast Release History:** available from flight data.
- **Location, Date and Time of Launch:** Trapani-Milo Launch Base – Aug. 20, 1995 – 05:34 UTC (07:54 local time).
- **Thermo-optical properties of the balloon film:** data provided by the manufacturer for the USV-FTB1 balloon, assuming that the balloon film is essentially the same.

5.3.3 – Results

Figure 5.4 and Figure 5.5 show the rate-of-climb GPS data and the altitude GPS data compared to simulation outputs.

It can be seen that ACHAB results (both *RoC* and altitude profile) are in reasonably good agreement with GPS data throughout the entire flight. It is evident, though, that the initial velocity is *overestimated* by the simulation tool. It must be pointed out that the exact value of the initial mass of gas for this case is unknown (no error evaluation on the loaded lifting force was provided).

Ballasting was simulated according the ballast release history provided with the data set.

Actually the Ballast Discharge List is the following:

$$BallastDischargeList = \begin{bmatrix} 0 & 0 \\ \vdots & \vdots \\ 3183 & 24.8 \\ 3542 & 24.8 \\ 4009 & 24.8 \end{bmatrix}$$

On the same figures there are 2 other simulations. The red line is SINBAD output with a drag coefficient of $C_d = 0.45$. It can be seen that SINBAD estimates a better value of the initial velocity, but in general it overestimates the rate of climb. The green line shows ACHAB simulation with a constant drag coefficient $C_d = 0.45$. As it can be seen, in this case, ACHAB underestimates the up velocity throughout the troposphere.

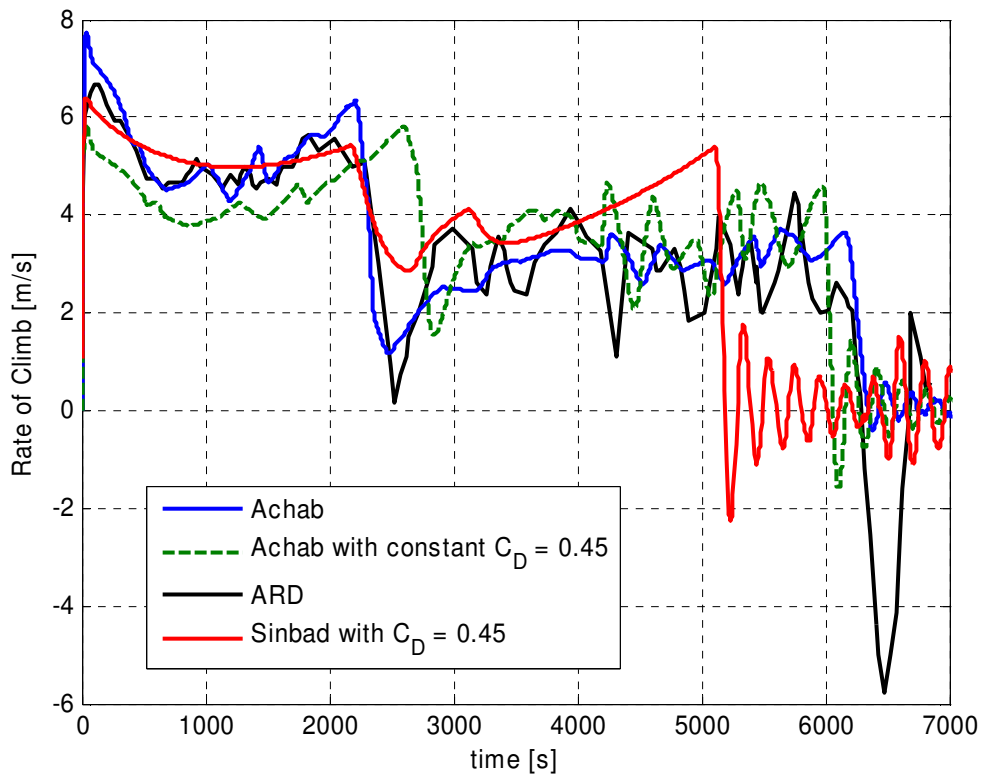


Figure 5.4 - ARD GPS rate of climb data compared to simulation outputs. GPS data were graphically extracted from printed plots.

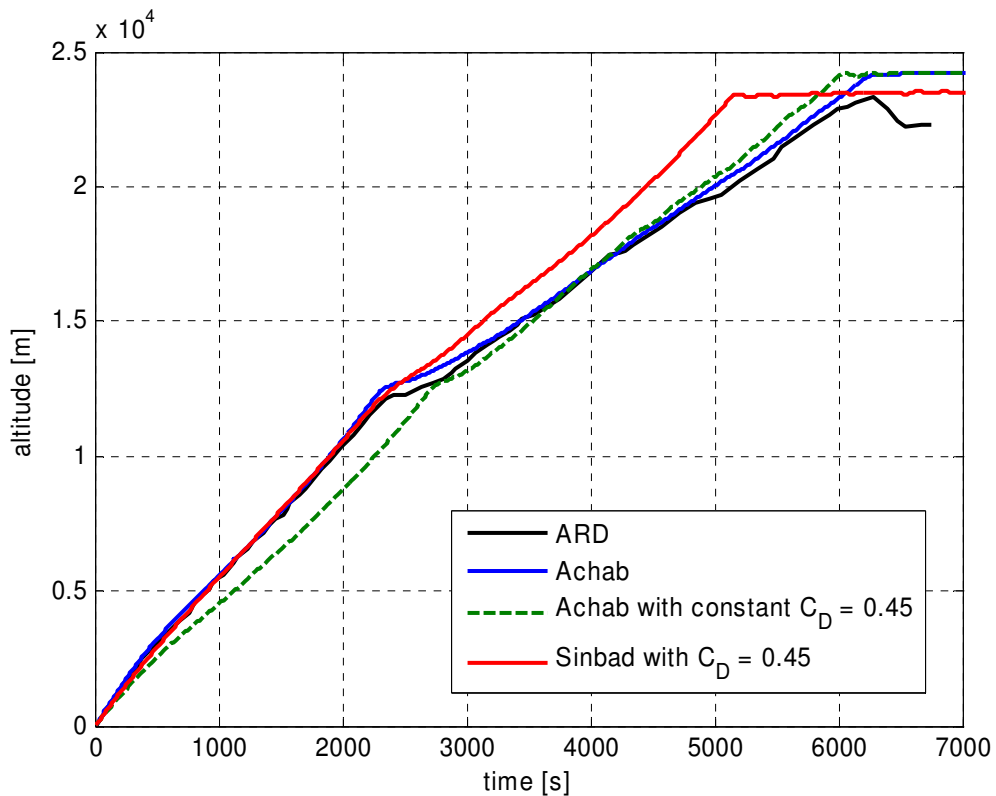


Figure 5.5 - ARD GPS altitude data compared to simulation outputs. GPS data were graphically extracted from printed plots.

As for the previous case, an *integral error* and the *rms* error evaluation was considered to give an indication of the performances of the simulation tools (Table 5.2).

Error [m/s]	Simulator	Tropospheric Flight Segment	Stratospheric Flight Segment	Global Flight
\bar{e}	ACHAB	0.17	-0.04	0.04
	SINBAD	0.10	0.17	0.15
<i>rms</i>	ACHAB	0.39	0.90	0.76
	SINBAD	0.343	1.96	1.58

Table 5.2 – Comparison of the performance indices for the two codes.

The *rms* error for SINBAD (in the stratospheric segment) is higher because its simulation attains the float altitude long before the real flight. As before, this is not evidenced by the integral error because, as it can be seen from Figure 5.4, the large discrepancy between SINBAD and the GPS rate of climb in the stratospheric segment is, *on average*, small.

It must be remarked that the available data were only on **printed paper format**, therefore the velocity and altitude data were extracted from printed plots.

Using the available data with a $C_d = 0.45$, the formula reported previously yields an initial steady velocity of:

$$V_{ssZ} \cong 6.1 \text{ [m/s]}$$

Again, this is valid when $T_{gas} = T_{air}$ and the upward acceleration is zero.

This value is apparently **below real flight data** and well below ACHAB's prediction (Figure 5.6).

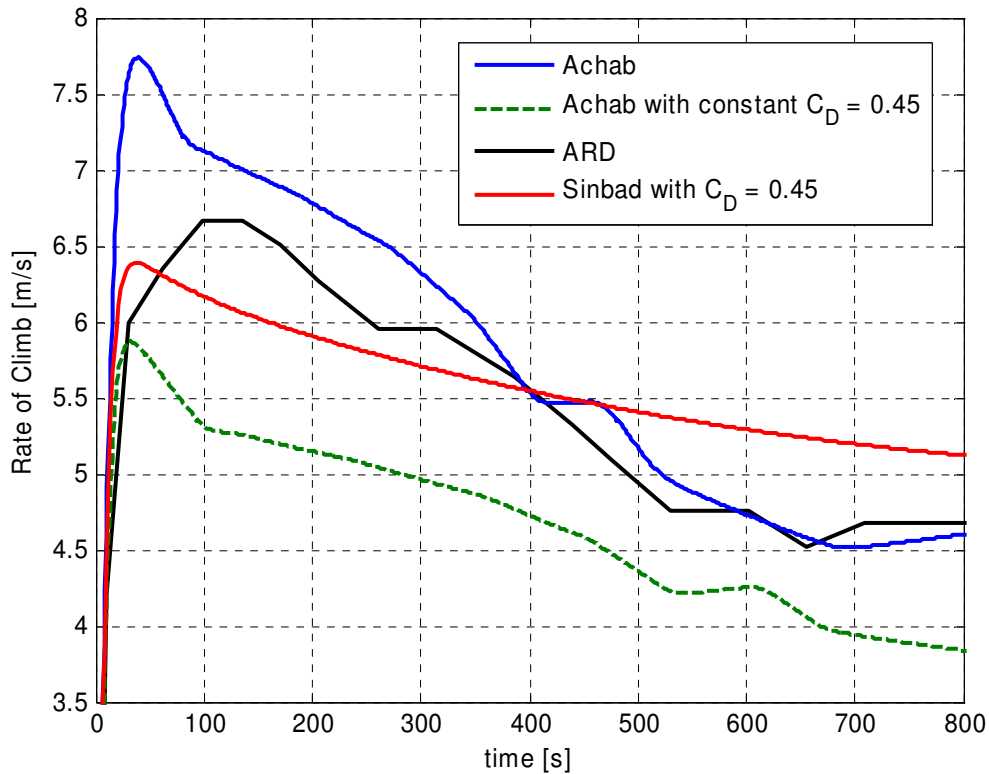


Figure 5.6 – Initial rate of climb.

5.4 – Validation Results

The validation of ACHAB has been performed by comparing simulation results to **experimental flight data** and to the outputs of a reference software, SINBAD.

The use of NASA’s SINBAD simulation tool can be justified by the fact that it is the most adopted simulation tool for balloon trajectory forecast in several launches all over the world and by many different organizations. Nevertheless, SINBAD reliability when used as balloon trajectory prediction tool is still under discussion (see Ref. 38). Various comparison of SINBAD results with actual data (Ref. 38, 39) show that it can be a good prediction tool only when some balloon characteristic parameters and atmospheric data have been preliminarily fine tuned with flight data. This means that at least one flight shall be performed with the same balloon in the same launch area to obtain good results. For instance, in the experimental cases at hand, SINBAD exhibits a mean error of 0.2 m/s and appears less accurate than ACHAB.

Comparisons between ACHAB and SINBAD using the same set of input parameters show that SINBAD typically tends to estimate an overall *RoC* greater than ACHAB leading also to early reaching of the float altitude. Typical *RoC* differences between the two tools are of the order of 1 m/s .

Conversely, comparison between ACHAB and actual flight data show that this tool is in **good agreement with experimental data** with mean error on the *RoC* of about 0.1 m/s.

The use of more experimental data would confirm the above error figures. Anyway, the validation process of ACHAB, at least demonstrates clearly the same SINBAD capability to be **a very accurate tool for balloon trajectory forecast** (even more accurate than SINBAD).

For this reason, the *Italian Aerospace Research Center* has considered ACHAB suitable for mission planning and trajectory prediction for the DTFT1 Balloon Flight, which will be discussed in the next chapter.

6

The USV-DTFT1 Balloon Flight

In this section the performance of ACHAB with respect to mission planning and trajectory prediction for the USV-DTFT1 Balloon flight will be discussed.

6.1 – Mission Planning

Before the beginning of the flight campaign for the DTFT1 mission, ACHAB was conveniently used for *mission planning* purposes. Actually the objective of the analysis was to verify and assess on the balloon flight feasibility using as launch base the Arbatax-Tortolì Airport, in Sardinia, Italy.

6.1.1 – Determining the Flight Envelope

Using atmospheric and wind profiles relative to the time period between October and March 2000-2006, more than 1000 trajectories of the DTFT1 ascent flight were simulated using ACHAB. This allowed to determine and trace a *flight envelope* for the nominal mission.

Figure 6.1 shows the trajectories that compose the nominal flight trajectories.

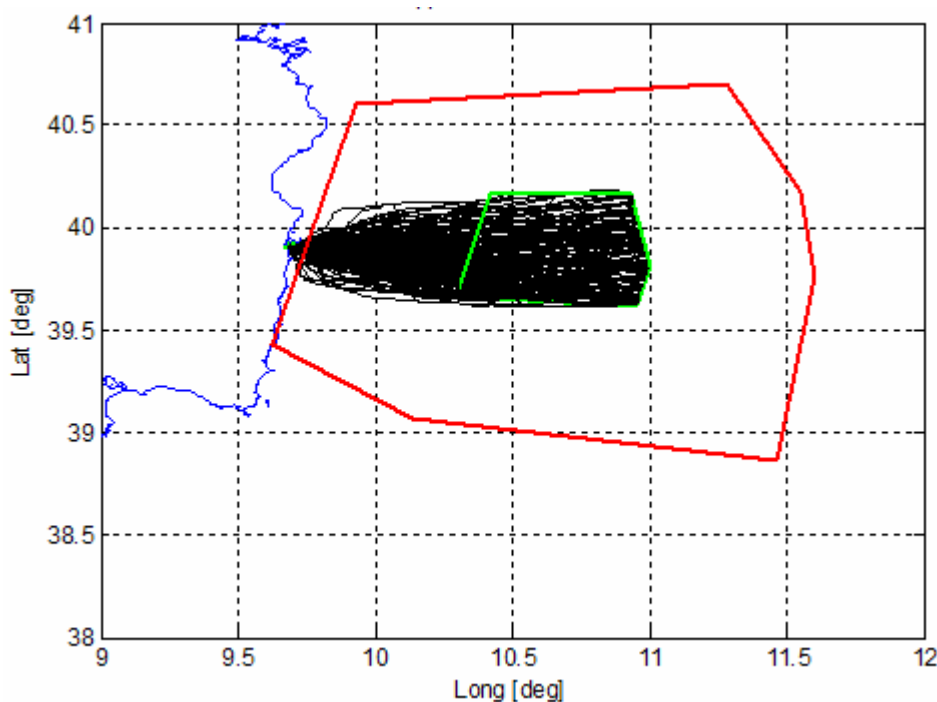


Figure 6.1 – Nominal Flight Envelope.

These trajectories represent almost 23% of those analyzed and were chosen because they comply with the following constraints:

- they head directly toward the sea without crossing any land
- they reach and/or cross the safe *Release Zone*

Analyzing the results of the simulations it was possible to state the feasibility of the flight from the airport of Arbatax-Tortolì.

Moreover it was also possible to statistically infer the monthly flight chances in the time period considered.

6.2 – Flight Analysis and Results

Throughout the USV-DTFT1 flight campaign, ACHAB was constantly used for trajectory prediction. Together with ECMWF weather forecast files⁴¹, ACHAB was run *daily* (with the aid of an *off-line optimization tool*, briefly discussed in Chapter 8) in order to decide if the following days were to be considered suitable for the balloon flight.

The last *trajectory bulletin* was issued on February 23, 2007, at -18 hours before the scheduled lift-off (07:00 UTC). Flight predictions were produced using the ECMWF_1218 weather and wind forecast data⁴¹.

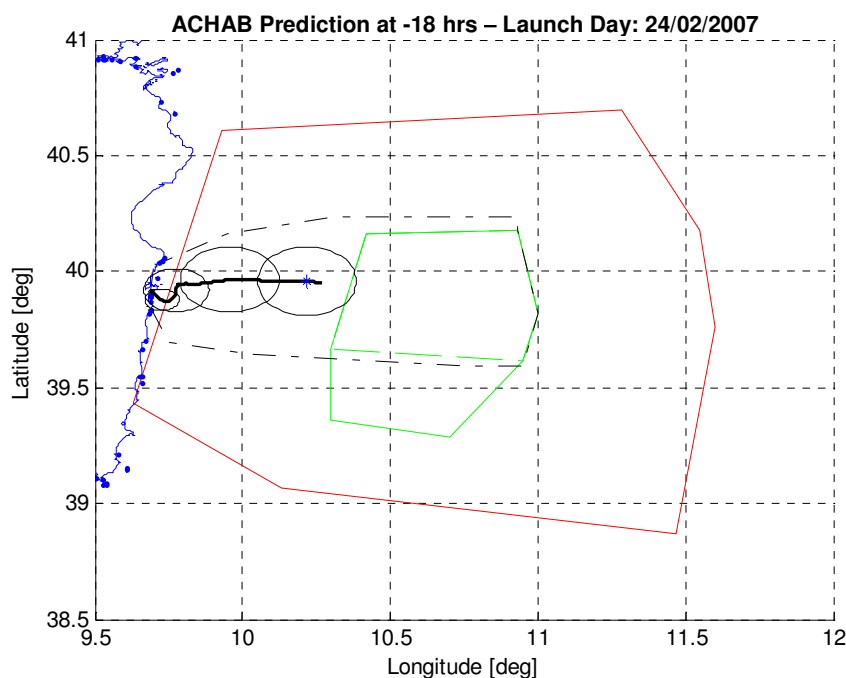


Figure 6.2 – DTFT1 Balloon flight prediction at -18 hrs before lift-off.

Even if the predicted trajectory (see Figure 6.2) did not reach exactly the *Release Zone* (see Chapter 2) the Mission Board **decided to operate the launch nominally** because it was verified that all of the system parts (Vehicle, Gondola, Balloon) would splashdown safely without being of any danger¹².

The balloon was inflated with a **nominal free lift of 10%**. Of course, as discussed in Chapter 4, the true value of the free lift was unknown at lift-off and could only be determined long after the flight.

In the following sections the performance of ACHAB will be evaluated comparing the GPS data of the real balloon flight (which took place on Feb. 24, 2007) with both the prediction data available *before the flight* and the *post-flight* analysis data (i.e. **accurate weather and atmospheric data, actual helium mass**).

6.2.1 – Input Data

Main characteristics of the system:

- **Balloon Maximum Volume:** 334711 m³
- **Balloon Mass:** 1433 kg
- **Payload Mass:** 2556 kg (no ballast)
- **Ballast:** 500 kg
- **Assumed Percentage Free Lift:** 10%
- **Assumed Lifting Gas Mass:** 791.8 kg (helium)
- **Actual Percentage Free Lift:** 10.95% **[determined during post-flight analysis]**
- **Actual Lifting Gas Mass:** 798.6 kg (helium) **[determined during post-flight analysis]**
- **Ground Air Temperature:** 282.15 K
- **Ground Air Pressure:** 101360 Pa
- **Location, Date and Time of Launch:**
- Arbatax Launch Base (Lat: 39.916367° - Long: 9.6882667°).
- February 24, 2007 – 07:30 UT (08:30 local time).
- **Thermo-optical properties of the balloon film:** data provided by the manufacturer for the USV-FTB1 balloon

These data together with the ECMWF **forecast** file and the ECMWF **analysis** file (after the flight) were used for pre-flight prediction and post-flight analysis.

6.2.2 – Prediction Performance at -18 hours before Launch

In order to quantify the performance of ACHAB's prediction with respect to the actual flight data using the flight prediction at -18 hours before launch (i.e. using the **ECMWF_1218 forecast** file and **10% free lift**), it is possible to use the performance indices introduced in Chapter 5: the *integral error* on the rate of climb and the *root-mean-square (rms) error* on the rate of climb. As previously done, these indices will

be evaluated in the two segments of the flight (tropospheric and stratospheric) and also for the global flight (Table 6.1).

Simulator	Error [m/s]	Tropospheric Flight Segment	Stratospheric Flight Segment	Global Flight
ACHAB	\bar{e}	0.02	0.25	0.16
	<i>rms</i>	1.30	2.28	1.96

Table 6.1 – ACHAB’s performance with respect to -18 hrs forecast data.

Concerning the trajectory prediction, it is possible to evaluate the error difference in % between the predicted trajectory and the actual trajectory in terms of latitude and longitude dispersion.

We have evaluated the following relative errors, for each altitude h , as a measure of the *relative gap* between the actual and the predicted trajectory:

$$\frac{\Delta Long(h)}{Long_{GPS}(h)} = \frac{Long_{ACHAB}(h) - Long_{GPS}(h)}{Long_{GPS}(h)}$$

$$\frac{\Delta Lat(h)}{Lat_{GPS}(h)} = \frac{Lat_{ACHAB}(h) - Lat_{GPS}(h)}{Lat_{GPS}(h)}$$

We have found that **for each altitude h** , the following inequalities are true:

$$\frac{\Delta Long(h)}{Long_{GPS}(h)} < 1\%$$

$$\frac{\Delta Lat(h)}{Lat_{GPS}(h)} \ll 1\%$$

In particular the error difference on the release point prediction with respect to the actual release point:

- error on latitude position: 0.02% (\cong 0.8 km)
- error on longitude position: 0.8% (\cong 7 km)

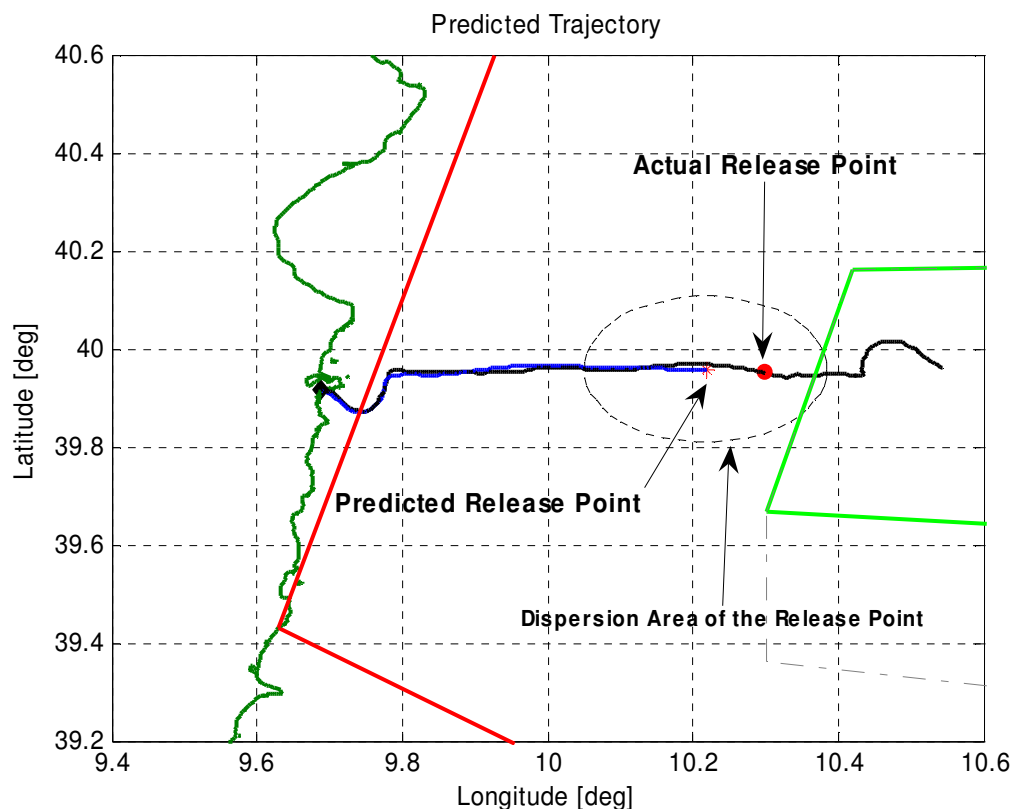


Figure 6.3 – Comparison between the actual trajectory and predicted trajectory using the -18 hrs forecast data.

6.2.3 – Post-Flight Analysis Performance

After the flight some input data are known with *better accuracy*. In particular, the **ECMWF analysis file** for the atmospheric data is available together with the measurement (in static conditions) of the remaining pressure inside the helium tanks. It was estimated that the amount of gas that was loaded inside the balloon at inflation (assuming that no gas was lost during inflation) was:

$$M_{gas0} = 798.6 \text{ kg}$$

This mass value corresponds to a free-lift of about 11%.

The **performance** of ACHAB was evaluated in the same manner as presented in the previous paragraph. In addition, a comparison between the performance of ACHAB and SINBAD was carried out in the same simulation conditions as far as possible. Of course this kind of performance comparison is not possible on north and east

components of the velocity neither it is possible on the horizontal trajectory prediction, because SINBAD computes **only** the vertical motion of the balloon.

As for the previous cases, an *integral error* and a *rms* error evaluation was considered to give a quantitative comparison between the tools.

Error [m/s]	Simulator	Tropospheric Flight Segment	Stratospheric Flight Segment	Global Flight
\bar{e}	ACHAB	0.12	0.54	0.38
	SINBAD	0.39	2.46	1.70
<i>rms</i>	ACHAB	0.88	0.99	0.95
	SINBAD	0.87	2.82	2.31

Table 6.2 – Comparison between ACHAB and SINBAD performances.

It might appear odd that the *integral errors* for the prediction at -18h are lower than those for the post-flight analysis. This is a consequence of the fact that in the prediction at -18h, actual gas mass was *underestimated* (because unknown), producing a lower rate of climb that, **on average** produces a lower *integral error*. However, as it can be seen, the **rms errors are higher** than those for the post-flight analysis, thus indicating a *worse average* profile matching.

Figure 6.4 shows the comparison between the actual vertical speed, ACHAB's predicted vertical speed (blue line) with post-flight input data and SINBAD's predicted vertical speed (red line). As said in Chapter 5, SINBAD works only with a (customizable) constant drag coefficient. We have used $C_d = 0.45$ (Ref. 39, 43).

It can be seen that the prediction of the initial rate of climb was underestimated by ACHAB.

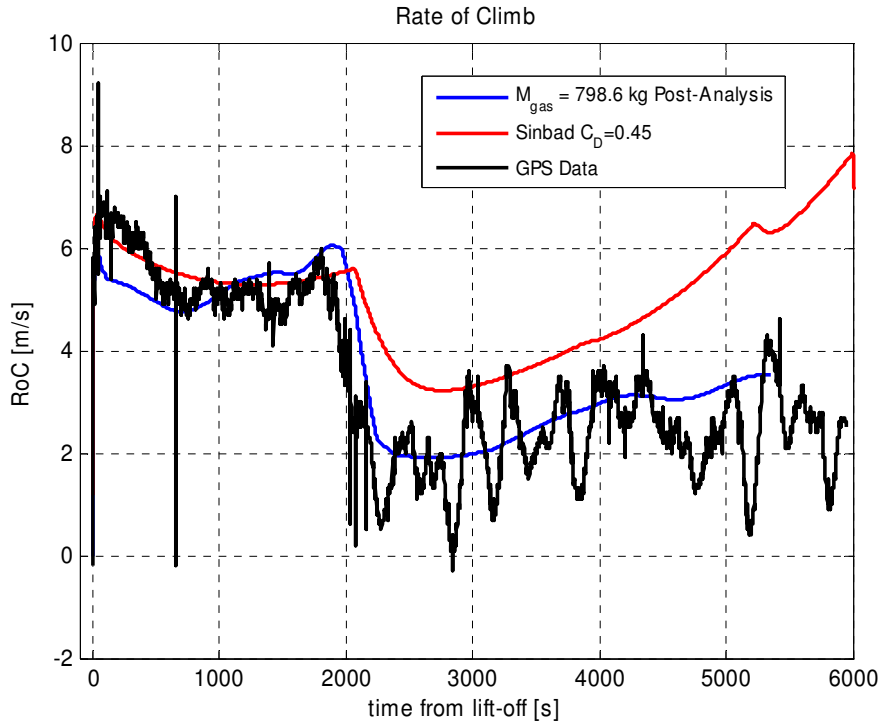


Figure 6.4 – Rate of climb comparison.

Figure 6.5 shows a comparison between actual and predicted North and East velocity components with post-flight input data.

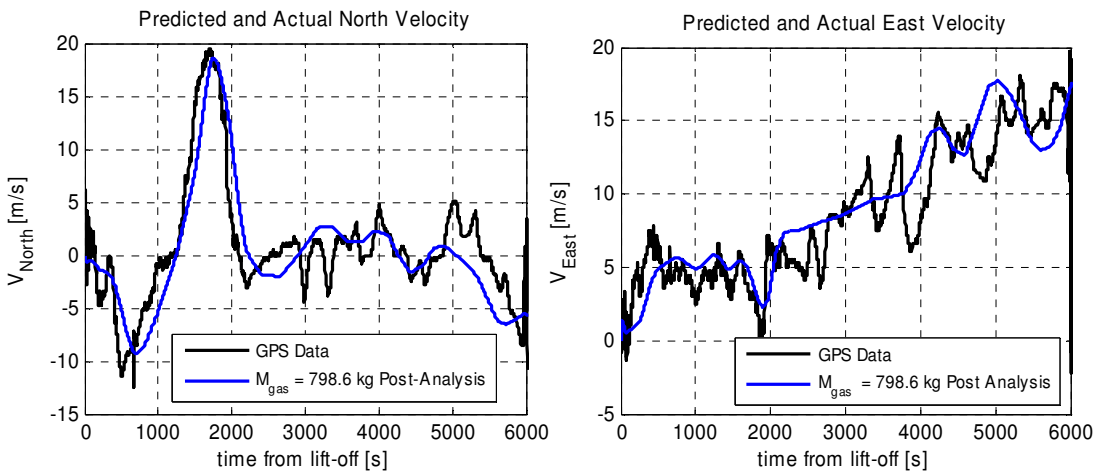


Figure 6.5 – Comparison between actual and predicted North and East velocity components with post-flight input data.

Finally, Figure 6.6 and 6.7 show the comparison between the actual trajectory and the predicted trajectory as computed by ACHAB using the available post-flight data.

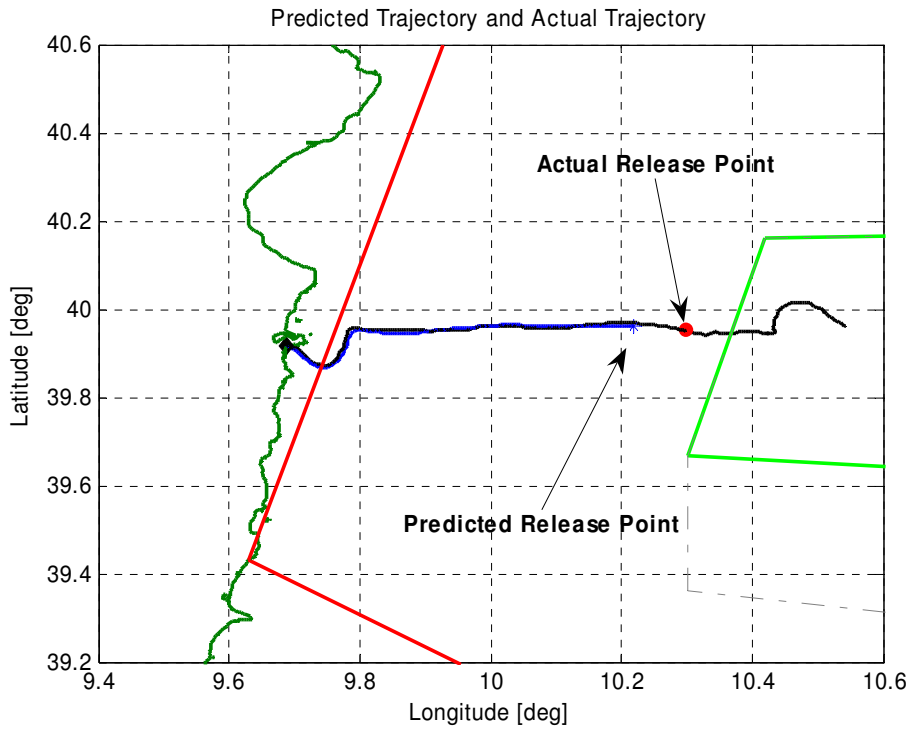


Figure 6.6 – Predicted (blue) and Actual (black) trajectory. The predicted trajectory was computed with actual gas mass and atmospheric data.

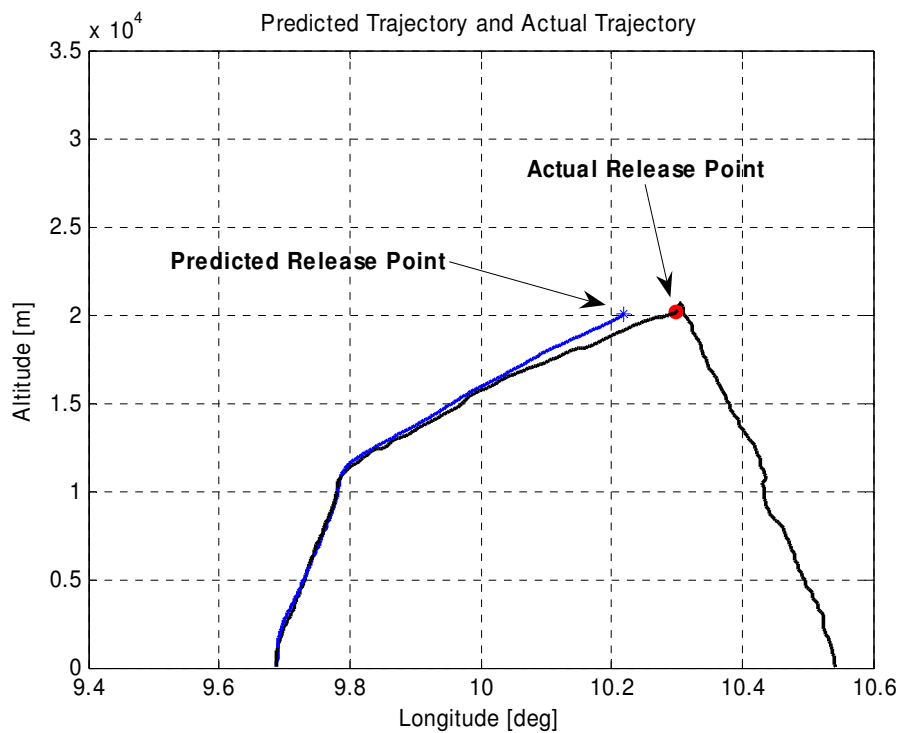


Figure 6.7 – Predicted (blue) and Actual (black) Longitude-Altitude Profile. The predicted trajectory was computed with actual gas mass and atmospheric data.

We have evaluated the following relative errors, for each altitude h , as a measure of the *relative gap* between the actual and the predicted trajectory:

$$\frac{\Delta Long(h)}{Long_{GPS}(h)} = \frac{Long_{ACHAB}(h) - Long_{GPS}(h)}{Long_{GPS}(h)}$$

$$\frac{\Delta Lat(h)}{Lat_{GPS}(h)} = \frac{Lat_{ACHAB}(h) - Lat_{GPS}(h)}{Lat_{GPS}(h)}$$

We have found that **for each altitude h** , the following inequalities are true:

$$\frac{\Delta Long(h)}{Long_{GPS}(h)} < 1\%$$

$$\frac{\Delta Lat(h)}{Lat_{GPS}(h)} \ll 1\%$$

Figure 6.8 and Figure 6.9 show the evolution of this relative error along the altitude.

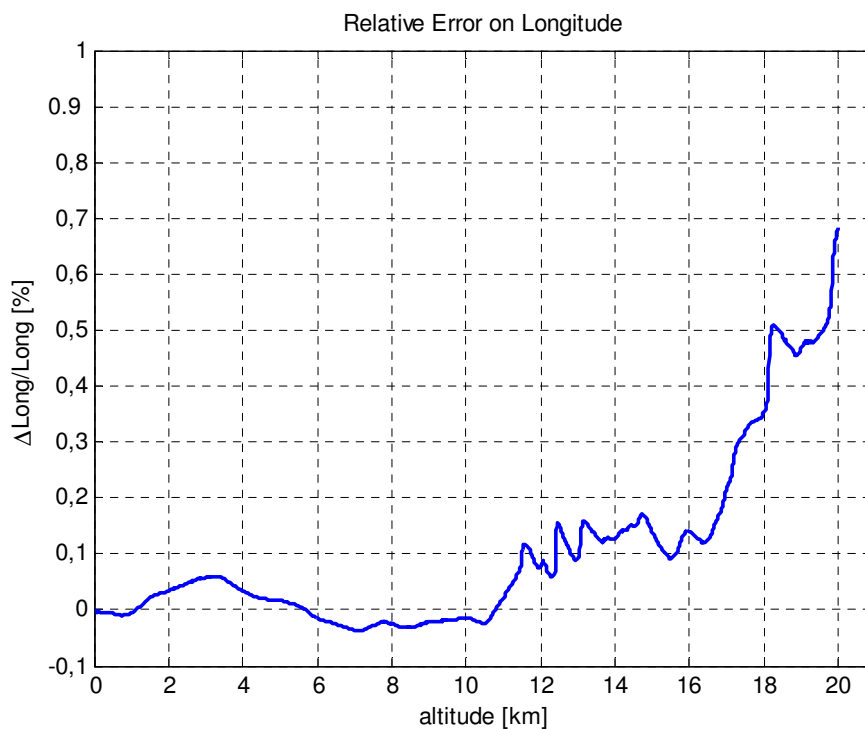


Figure 6.8 – Percentage relative error on longitude.

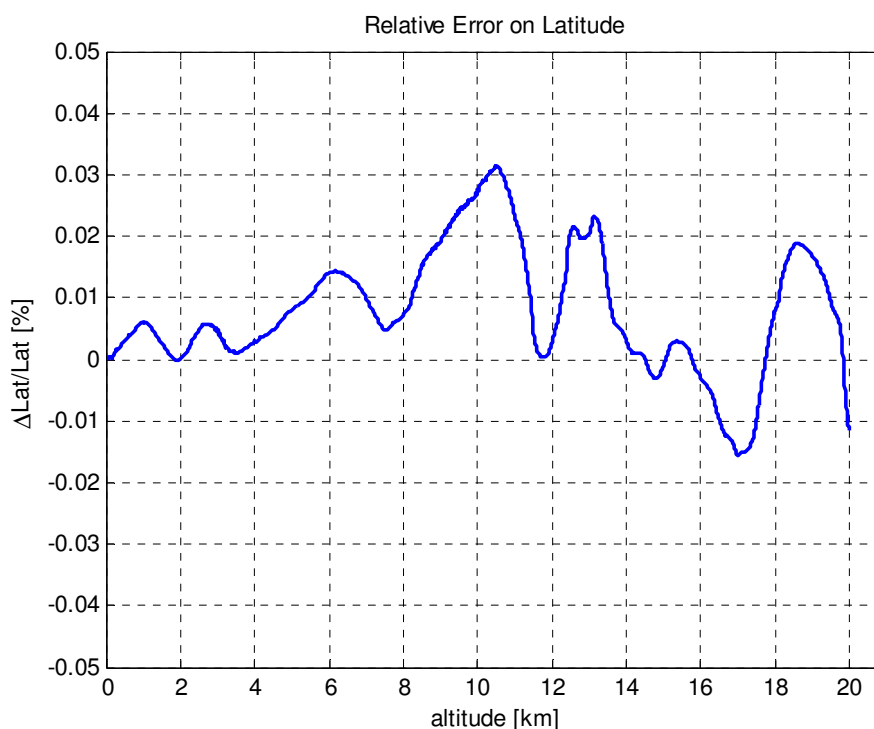


Figure 6.9 – Percentage relative error on latitude.

As it can be seen from the figures, the error difference on the **release point prediction** is:

- error on latitude position: 0.02% (\cong 0.8 km)
- error on longitude position: 0.8% (\cong 7 km)

6.3 – Final Considerations

The post-flight analysis has evidenced some advantages and some limitations of the prediction tool at our disposal.

The analysis on ACHAB has actually confirmed:

- the capability to be an accurate tool for balloon trajectory forecast (even more accurate than SINBAD) with mean error on the *RoC* less than 0.5 m/s.
- the capability to predict the trajectory with relative errors on latitude and longitude less than 1%
- the validity of the ECMWF forecast data for horizontal trajectory prediction

Thus, it is evidenced that the overall performance of ACHAB is **largely satisfying**.

Nonetheless the analysis has shown that:

- the initial rate of climb was substantially different between the predicted data and the flight data
- the fact that the gas mass is *not precisely known* at lift-off could lead to inaccurate estimates of the rate of climb of the balloon and it is, as expected, the major cause of prediction inaccuracy

As a matter of fact, the error on the *release point position* is largely due to:

- the *rate of climb differences* between the predicted data and the flight data.
- possible unmodeled thermal effects due to the *presence of clouds*
- the uncertainties on the horizontal wind velocity (differences between the actual winds and the ECMWF data)
- modeling of the horizontal drag acting on the balloon



7

Lessons Learned from the USV-DTFT1 Mission

The purpose of this section is to present some of the lessons learned during the DTFT1 Balloon Flight and to present the possible improvements that are currently being implemented in ACHAB.

7.1 – Lessons Learned

The post-flight analysis of the DTFT1 Balloon Flight has certainly confirmed the *merits* and the *value* of ACHAB, but has also evidences some *limitations*.

Actually, the analysis has shown that:

- the *initial rate of climb* was substantially different between the predicted data and the flight data; in particular it was underestimated;
- the *release point* was predicted with an error of about 7 km in longitude, even when using the post flight analysis input data.

These facts indicate that there are still some modeling aspects of the simulation tool that need further investigation.

After a preliminary analysis, it was acknowledged²⁶ that the underestimation of the initial rate of climb was most probably due to an **overestimation of the drag coefficient**. Indeed, right after lift-off, aerodynamic effects are certainly predominant compared to thermodynamic effects on the balloon dynamics. Future activity will, therefore, focus on a **revision or at least on a refinement** of the *drag coefficient variability law* that was discussed in Chapter 3.

The underestimation of the initial vertical velocity can be considered, of course, one of the reasons for the error on the release point prediction, even if its incidence on the altitude profile is on average very small.

However, we believe that the main reason for the error on the release point prediction is to be found in the weather conditions in which the balloon flight took place²⁶. The USV-DTFT1 lift-off and ascent phase occurred under **partial cloud cover conditions** (see Figure 7.1). ACHAB is not currently able to simulate flights in *non-clear sky* conditions and it was validated using test cases flown on *clear sky* days only.

The presence of clouds can **certainly and significantly modify** the thermal environment in which the balloon moves. This may have caused a slower ascent rate in the stratospheric segment of the flight, determining eventually an eastwards shift of the release point .

In the next section a brief description of cloud cover effects on thermal environment (as far as balloon flight is concerned) will be given in order **to set the background for future enhancements of the code**.

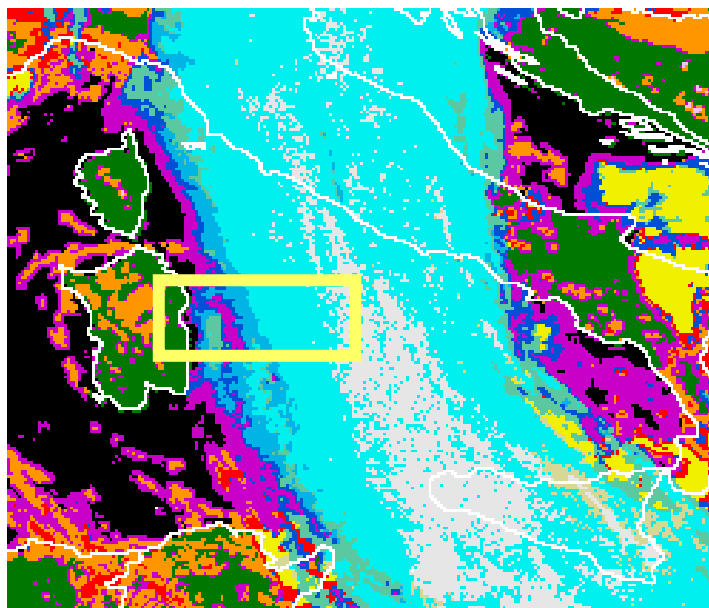


Figure 7.1 – Cloud cover conditions during the ascent phase of the DTFT1 flight. Cloud cover was mainly due to *stratus* clouds (Image from Ref. 44).

7.2 – Effects of Clouds on Thermal Fluxes

As previously stated (see Chapter 3), it is very important to carefully consider the surrounding thermal environment in which the balloon moves. Therefore, if the balloon flight does not take place on a clear day, the presence of clouds must be taken into account. It is important to remark though, that it is good ballooning practice that launches must never occur during cloudy days.

Clouds significantly modify the thermal environment^{9,34,35} in which the balloon flies. Their presence have an effect on some of the thermal fluxes defined earlier.

In particular, the fluxes affected are:

- the direct solar flux
- the albedo flux
- the thermal flux from ground

More in details, depending upon the *relative altitude* of balloon and clouds, and on *cloud cover fraction*, different effects must be considered. In addition different kinds of clouds have different impacts on the balloon, because of their different transparency to radiation.

Figure 7.2 shows, in summary, cloud cover effects on the thermal environment.

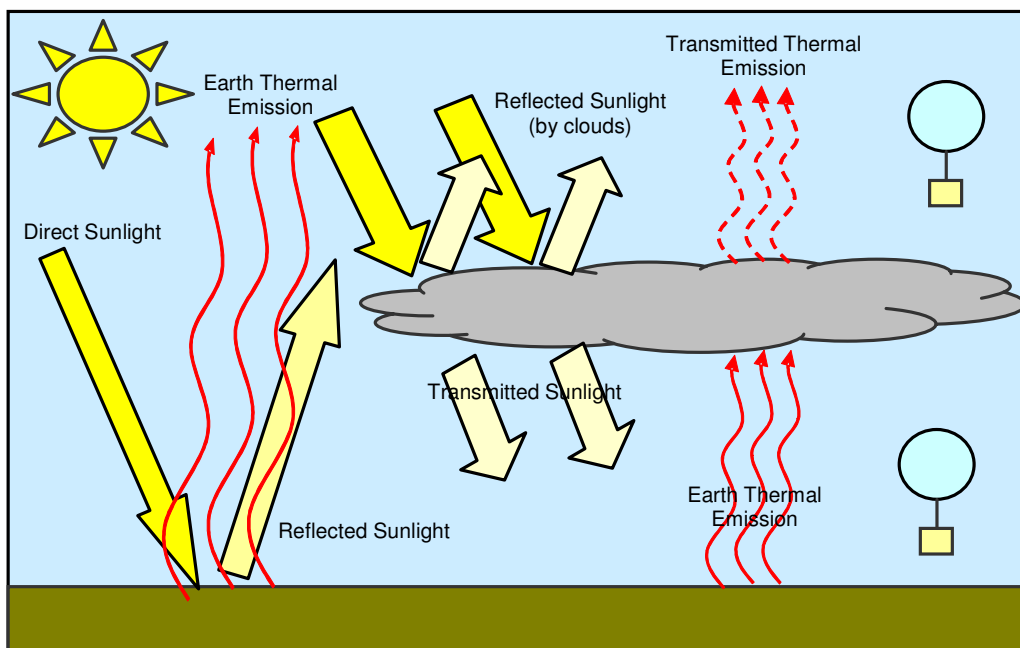


Figure 7.2 – Effects of clouds on thermal fluxes.

Below the cloud layer, the balloon is exposed to the direct sunlight only for a fraction, while the rest of it is obscured by the cloud layer. However, clouds, depending on their kind (*low, middle* or *high*), have a certain degree of transparency which can be quantified through their transmissivity coefficient (in the shortwave and longwave spectrum). Therefore there is a certain amount of attenuated sunlight that reaches the balloon.

Above the cloud layer the balloon is totally exposed to the direct sunlight, so no heat flux modification will occur.

Obviously the presence of clouds also modifies the albedo thermal flux since part of the sunlight is obscured and therefore only a fraction of it will be reflected by the surface. For altitudes higher than the cloud layer it is important to consider also a mean value of the cloud reflectivity coefficient (that roughly depends on the kind of cloud considered).

Finally, the presence of clouds acts as a screen for the infrared radiation coming from the Earth surface. For this reason when the balloon is above the altitude of clouds, the longwave thermal flux will be partially transmitted through the cloud layer.

8

ACHAB Related Projects

In this chapter a brief description of some of the main projects and tools that originated from ACHAB will be given. These activities are currently carried out at the *Italian Aerospace Research Center*.

8.1 – ACHAB Related Projects

The development of ACHAB has allowed the design of several advanced decision-making tools that proved to be extremely useful during the flight campaign of the DTFT1 Mission.

In the following sections, the major projects – carried out entirely by the *Italian Aerospace Research Center (CIRA)* – will be briefly introduced. The present author

has actively participated to the realization of most them but evidently they are *not* part of this Ph.D. thesis. They are mentioned here only for completeness and in order to report some of the applicative outcomes that derived from ACHAB.

8.2 – SANBA: The Balloon Navigation Facility

SANBA (System for Augmented Navigation of BALloon missions) is a real-time online navigation facility that integrates several prediction and decision-making tools extremely useful during balloon flight missions⁴⁵. It is also able to acquire the GPS data coming from the balloon gondola and is able to display the trajectory and the current position on a map. Figure 8.1 shows a global view of SANBA graphical user interface.

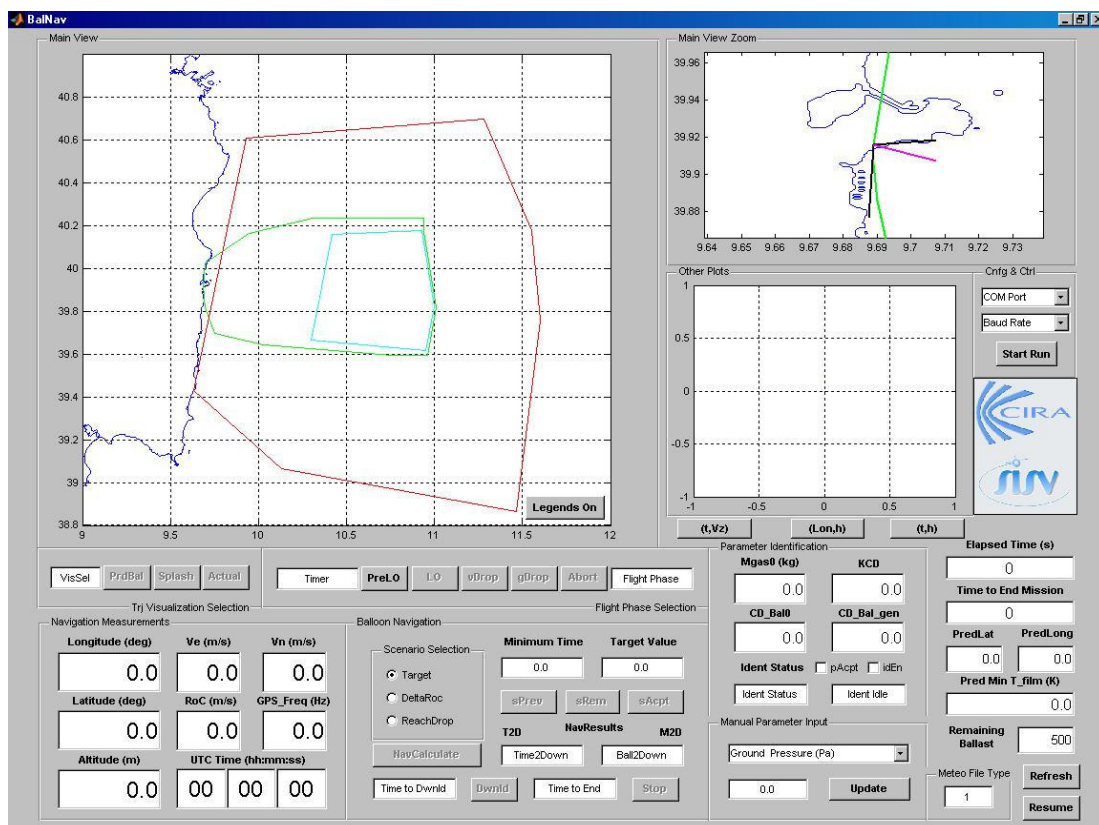


Figure 8.1 – SANBA graphical user interface.

SANBA has different modules with several features and functionalities that make it a unique navigation tool. The main modules are described in the following list⁴⁵:

- **MAIN**: the management module that handles the Modules and Functions Scheduling, the External and Internal Communication Functions, Time Services, MMI Data Exchange, Recovery Functions.
- **ACHAB**: the Analysis Code for High-Altitude Balloons described in the present work. ACHAB was interfaced with SANBA in order to allow **on-line flight trajectory prediction and visualization** of zero-pressure balloons and indeed represents the *core* of the prediction, optimization and identification modules (see following list items).
- **Optimize_Trj**: an online optimization tool capable of finding (by iteratively calling ACHAB), optimal ballast drop maneuvers in order to maximize the probability to reach the *Release Zone*.
- **Bal_Ident**: an identification tool, aimed at finding the “exact” value for relevant parameters that are, in contrast, usually known with uncertainty in order to improve the online trajectory prediction. For example the **inflated gas mass**, determined, as a rule, from indirect measurements of temperature and pressure of the residual gas in the tanks after balloon inflation, and so known only within a confidence level; or the **balloon drag coefficient**, hard to evaluate because of the changes of the balloon size and shape during the ascent, especially the first part. The time domain approach, based on the output error method, is used to perform balloon parameters estimation. Also in this case existing limits on the parameters to be identified are incorporated in the problem, that is solved using a constrained Gauss-Newton method.
- **ID_ACHAB**, i.e. ACHAB for parameter identification purposes. The main difference between ACHAB and ID_ACHAB is relating to the different data management, associated to the objective of identification, that is a function of the actual carrier flight phase.
- **SplashDownSim**: a parachuted descent simulator, used to predict the splashdown point for both the payload of the balloon and the balloon itself.

Figure 8.2, taken from Ref. 45, shows the overall architecture of SANBA.

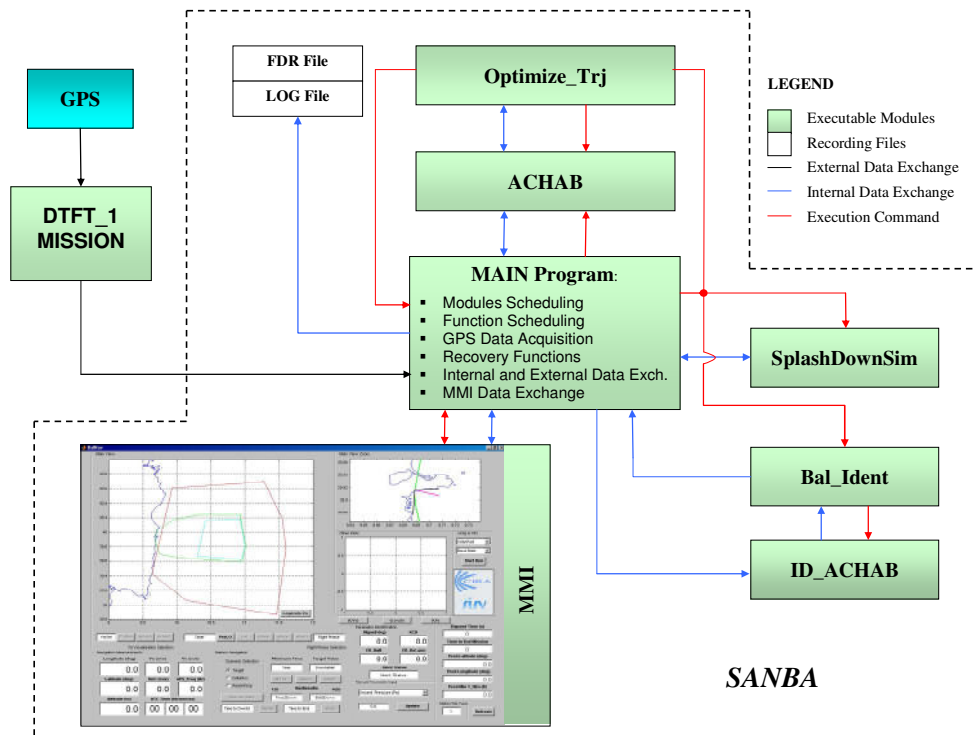


Figure 8.2 – SANBA architecture (Ref. 45).

SANBA was successfully used during the DTFT1 Balloon Flight, allowing complete tracking and on-line prediction of the balloon flight and complete control of the mission status.

8.3 – Balloon Mission Optimization Facility

Another important decision-making tool for balloon flight preparation and planning, was the Balloon Mission Optimization Facility. This off-line software allows to determine the optimal helium mass (or free-lift) to be charged into the balloon in order to maximize the probability to reach the *Release Zone*. The optimization process calls iteratively ACHAB with the objective of maximizing a probability function determined by means of a statistical analysis of the wind forecast data available for the flight zone.

Figure 8.3 shows the graphical user interface of the software.

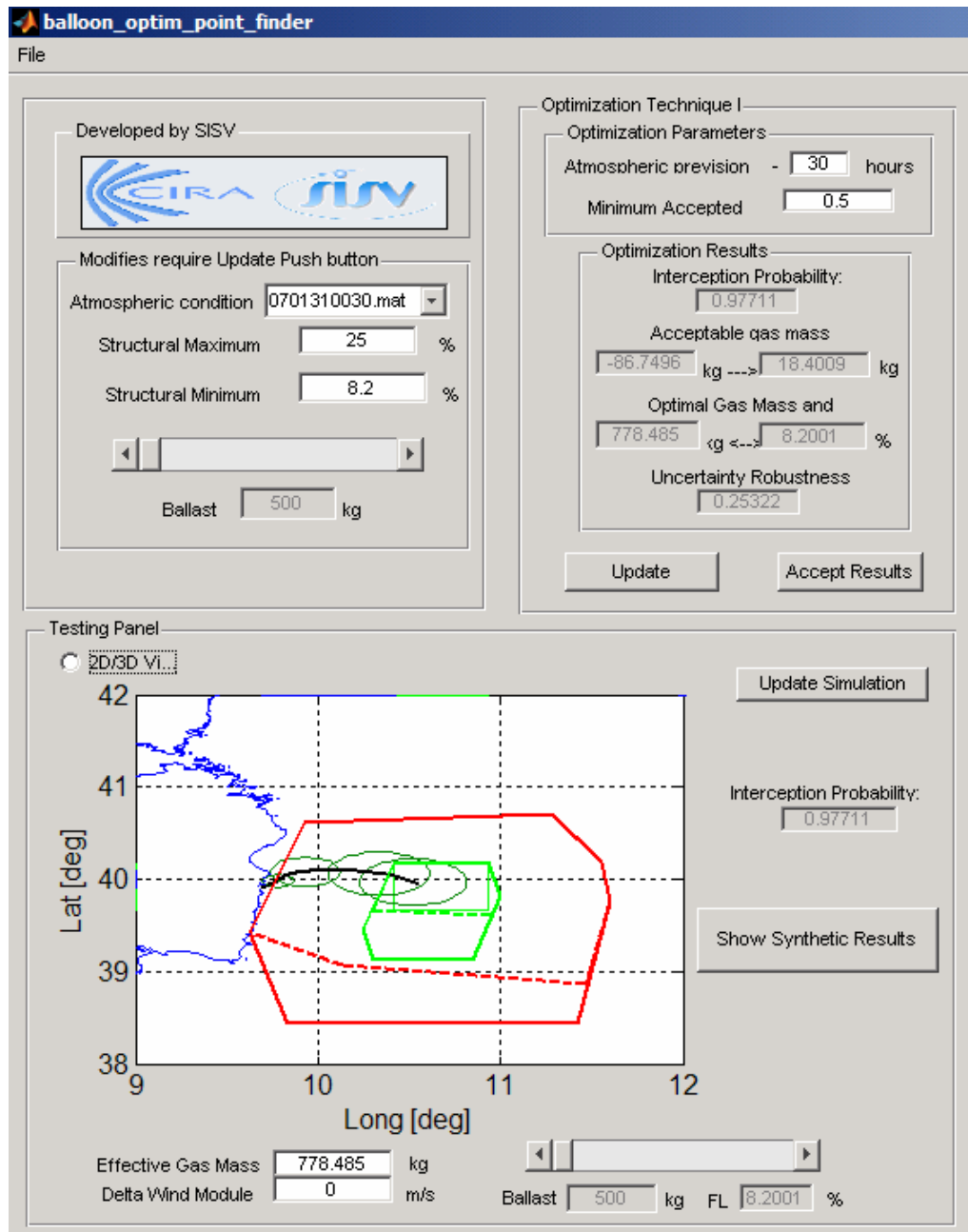


Figure 8.3 – The balloon mission optimization facility MMI.

This off-line optimization tool gives several synthetic results including:

- optimal free-lift (and gas mass)
- the probability to reach the zone
- 2D and 3D trajectory plots including dispersion areas as a function of the forecast files

The balloon mission optimization facility was successfully used for mission preparation and planning during the flight campaign of the DTFT1 Mission.

8.4 – Other Applications

Balloons have already have been useful in *planetary research* for testing systems that would be used later in space^{47,40}. They have also been used in *planetary exploration* missions^{47,48}. And many applications in this field are foreseen in the near future, especially concerning *Mars* and *Titan* exploration^{47,46}.

In this context, ACHAB could be easily reused for extra-terrestrial mission planning, because, thanks to its modularity, it allows an easy swap between atmospheric characteristics and/or planetary characteristics.

In addition, the thermal model developed for ACHAB is not limited to zero-pressure balloons but it can be used also (with minor modifications) for the simulation of super-pressure balloons, airships or other LTA systems.

9

Conclusions and Future Work

This chapter presents the conclusions and the future work upon which upcoming activities concerning this research will focus on.

9.1 – Conclusions

In this work we have presented the *theoretical bases*, the *development process*, the *validation* and the *experimental application* of the software **ACHAB** (**A**nalysis **C**ode for **H**igh-**A**ltitude **B**alloons), a simulation model for trajectory forecast, performance analysis and aerospace mission planning with high altitude zero pressure balloons.

ACHAB was primarily developed in support of the activities of CIRA's PRORA-USV Project, in order to fulfill the requirements of the first missions of the USV-

FTB_1 experimental vehicle, that use a stratospheric balloon as carrier system. Indeed ACHAB was successfully used for trajectory prediction during the flight campaign of the DTFT1 Mission by the Italian Aerospace Research Center.

ACHAB has been validated (Chapter 5) comparing simulation results with recorded GPS data of different balloon flights and it was also compared to the outputs of a reference software, SINBAD v3.1G (NASA's Scientific Balloon Analysis Model).

Performance evaluation on ACHAB has shown, during both validation process and post-flight analysis:

- the capability of the software to be an **accurate** tool for balloon trajectory forecast with a mean error on the *vertical velocity* less than 0.5 m/s.
- the capability of the software to predict the trajectory with relative errors on latitude and longitude dispersion less than 1%

Thus evidencing that the overall performance of the prediction tool is largely **satisfying**.

Nonetheless, the analysis has also shown some limitations of the software, that came up during the DTFT1 balloon flight (Chapter 6):

- the **initial** rate of climb was substantially different between the predicted data and the flight data; in particular it was underestimated
- the *release point* was predicted with an error of about 7 km

These facts indicate that there are still some modeling aspects of the simulation tool that need further investigation (Chapter 7).

Post-flight considerations have, however, acknowledged that:

- the underestimation of the initial rate of climb was most probably due to an **overestimation of the drag coefficient**, thus, suggesting a review or, at least, a refinement of the drag coefficient variability law
- the error on the release point prediction is to be found mostly in the weather conditions in which the balloon flight took place. Actually the USV-DTFT1 lift-off and ascent phase occurred under **partial cloud cover conditions** and

ACHAB is not currently able to simulate flights in *non-clear* sky conditions and it was validated using test cases flown on *clear sky* days only.

Future releases of ACHAB will be aimed at enhancing the performance of the prediction by taking into consideration the limitations and the effects listed above.

9.2 – Future Work

The development of ACHAB is still in progress. In particular future activities will focus on improving the prediction capabilities, trying to overcome the limitations evidenced by the post-flight analysis. In addition, there are several aspects concerning especially the thermal environment computation that can be modeled in a more detailed way.

The following list reports the main model improvements that can be considered as part of the future investigation and work:

- **Further investigation on drag coefficient variability law.**
- **Modelization and implementation of the thermal environment in the presence of clouds.**
- **Enhancement of the valving management system.**
- **Introduction of a variable albedo according to surface characteristics.**
- **Investigation on possible modeling of balloon buoyancy oscillations⁴².**
- **Gas leakage (at float altitude) due to film porosity.**
- **Implementation of ground emissivity ε_{ground} as a function of surface characteristics and day/night cycle.**

Acknowledgments

I am deeply grateful to Professor Michele Grassi and to Ing. Federico Corrado for their *guidance, encouragement* and *continuous support* throughout the development of this work.

My special thanks go to CIRA and especially to my fellow co-workers of the Flight Systems Department (SISV) involved in the PRORA-USV Project. Their collaboration, support and advice were inspiring and decisive in bringing ACHAB to life.

References

- [1] Crouch, T. D., "Lighter-than-air – An Overview", URL: <http://www.centennialofflight.gov/> [cited November 2007]
- [2] Pommereau, J-P., "Balloons, tools for investigating the stratosphere" - The middle atmosphere and space observations, International Summer School on Space Physics, Marseille, France, Aug. 1990. pp. 517-534. 1991
- [3] Picture from website, by Hock, T., "Drifting onto the scene" – URL: <http://www.ucar.edu/communications/quarterly/fall06/driftng.jsp> [cited November 2007]
- [4] "Early Scientific Balloons", URL: <http://www.centennialofflight.gov/> [cited November 2007]
- [5] Voss, L., "Scientific Research Using Balloons in the First Part of the Twentieth Century", URL: http://www.centennialofflight.gov/essay/Lighter_than_air/science-I/LTA14.htm [cited November 2007]
- [6] Voss, L., "Scientific Use of Balloons in the Second Half of the Twentieth Century", URL: http://www.centennialofflight.gov/essay/Lighter_than_air/Science_Missions-20th-Part_II/LTA15.htm [cited November 2007]
- [7] "Stratospheric balloons, history and present" – URL: <http://stratocat.com.ar/> [cited November 2007]
- [8] Suwal, K. R., "An Improved Balloon Venting Model" – AIAA-1986-2430, 1986.
- [9] Morris, A., editor, "Scientific Ballooning Handbook" – NCAR TN/1A-99, National Center for Atmospheric Research, Boulder CO, 1975.
- [10] Russo, G., "USV Flying Test Beds For Future Generations LV Technology Development" – AIAA 2003-6978
- [11] USV Program website, Centro Italiano Ricerche Aerospaziali CIRA – URL: http://www.cira.it/usv/usv_eng.asp/ [cited Novembre 2007]
- [12] Russo, G., "USV First Flight Results" – URL: http://www.cira.it/html/italiano/news/DTFT_1_1.pdf [cited October 2007]
- [13] Russo, G. "PRORA-USV: more Aeronautics in Space" – 1st International Convention of Technologies of the Frontier - The global importance of the incoming Space Economy, Medieval Castle of Moncrivello (VC) - April 1st 2006
- [14] Russo, G. (2007) Flight Test Experiments Foreseen for USV. In *Flight Experiments for Hypersonic Vehicle Development* (pp. 12-1 – 12-38). Educational Notes RTO-EN-AVT-130, Paper 12. Neuilly-sur-Seine, France: RTO.
- [15] Sabatano R., Filippone E., Russo M., **Palumbo R.**, "PRORA USV1: Safety Analysis and Splashdown Area Definition for the First USV Mission", AIAA-2006-8016, 14th AIAA/AHI International Space Planes and Hypersonics Systems and Technologies Conference, 6-9 November 2006, Canberra, Australia.
- [16] Kreith, F., Kreider, J. F., "Numerical Prediction of the Performance of High Altitude Balloons" – The Goddard Library: Balloon Technology Database: BT-1162, 1974.

- [17] Carlson, L. A., Horn, W. J., “A Unified Thermal and Vertical Trajectory Model for the Prediction of High Altitude Balloon Performance” – Texas Engineering Experiment Station Report TAMRF-4217-81-01, 1981.
- [18] Carlson, L. A., Horn, W. J., “New Thermal and Trajectory Model for High-Altitude Balloons” – *Journal of Aircraft*, Vol. 20, No. 6, 1983, pp. 500-507.
- [19] Raqué, S. M., Robbins, E. J., “Recent Developments in the SINBAD Balloon Vertical Performance Model” – AIAA 94-0517, 1994.
- [20] Farley, R. E., “BalloonAscent: 3D Simulation Tool for the Ascent and Float of High Altitude Balloons” – AIAA-2005-7412, 2005.
- [21] Stefan, K., “Performance Theory for Hot Air Balloons” – *Journal of Aircraft*, Vol. 16, No. 8, 1979, pp. 539-542.
- [22] Das, T., Mukherjee, R., Cameron, J., “Optimal Trajectory Planning for Hot-Air Balloons in Linear Wind Fields” – *Journal of Guidance, Control and Dynamics*, Vol. 26, No. 3, 2003.
- [23] Andersen, W. J., Shah, G. N., et al., “Added Mass of High-Altitude Balloons” – *Journal of Aircraft*, Vol. 32, No.2, 1995, pp. 285-289.
- [24] Dwyer, J. F., “Factors Affecting the Vertical Motion of a Zero-Pressure, Polyethylene, Free Balloon” – Air Force Geophysics Laboratory - AFGL-TR-85-0130.
- [25] Dudley Fitz, C., Hubbard, R. R., “Determination of Coefficient of Drag for a 530,000 Cubic Foot Natural Shape Balloon” – The Goddard Library: Balloon Technology Database: BT-1173, 1974.
- [26] **Palumbo, R.**, Russo, M., Filippone, E., Corrado, F., “ACHAB: Analysis Code for High Altitude Balloons” – AIAA-2007-6642.
- [27] Cathey, H. M., “Transient Thermal Loading of Natural Shaped Balloons” – AIAA-1997-31338.
- [28] Orr, G. D., “Atmospheric and Radiation Effects on Balloon Performance: A Review and Comparison of Flight Data and Vertical Performance Analysis Results” – AIAA-1997-31339.
- [29] Lienhard, J. H. IV, Lienhard, J. H. V, “A Heat Transfer Textbook” – Ebook - Phlogiston Press, Version 1.05, June 2002.
- [30] Mastrullo, R., Mazzei, P., Naso, V., Vanoli, R., “Fondamenti di Trasmissione del Calore”, Liguori Editore, 2001.
- [31] U.S. Naval Observatory – URL: <http://aa.usno.navy.mil/> [cited December 2006]
- [32] Earth Orbit Environmental Heating – NASA Goddard Space Flight Center, GUIDELINE NO. GD-AP-2301.
- [33] Payne, R. E., “Albedo of the Sea Surface” – *Journal of the Atmospheric Sciences*, Volume 29, Issue 5 (1972), pp. 959–970.
- [34] National Oceanic & Atmospheric Administration (NOAA) – <http://www.noaa.gov/>
- [35] NASA Langley Research Center's Clouds and the Earth's Radiant Energy System (CERES) Surface Properties Page – <http://www-surf.larc.nasa.gov/surf/>
- [36] Weismann, D., “A New Brittleness Criterion for Low Density Polyethylene Balloon Films” – The Goddard Library: Balloon Technology Database: BT-1041.29, 1972.

- [37] Weismann, D., “The Influence of Changes of Material Structure on the Failure of Polyethylene Balloon Films” – The Goddard Library: Balloon Technology Database: BT-1040.15, 1970.
- [38] Garde, G. J., “Comparison of Two Balloon Flight Simulation Programs” – AIAA-2005-7413.
- [39] Musso, I., Cardillo, A., Cosentino, O., Memmo, A., “A balloon trajectory prediction system” – *Advances in Space Research* 33 (2004), pp. 1722–1726.
- [40] Center of Studies and Activities for Space (CISAS), “HASI Stratospheric Balloon Experiments” – URL: http://cisas.unipd.it/balloon_HASI.htm [cited November 2007]
- [41] European Centre for Medium-Range Weather Forecasts – URL: <http://www.ecmwf.int/>
- [42] Anderson, W. J., Taback, I., “Oscillation of High-Altitude Balloons” – *Journal of Aircraft*, Vol. 28, No. 9, pp. 606-608.
- [43] De Giorgis, M., Borriello, G., Allasio, A., Vavala, R., Leveugle, T., Cosentino, O., “Atmospheric Reentry Demonstrator Balloon Flight Test” – *Journal of Spacecraft and Rockets*, Vol. 36, No. 4, July-August 1999.
- [44] Servizio Meteorologico dell’Aeronautica Militare – URL: <http://www.meteoam.it/>
- [45] Lai C., Cuciniello G., Nebula F., **Palumbo R.**, Russo M., Vitale A., Corrado F., “A Stratospheric Balloon Integrated Navigation Facility”, 18th ESA Symposium on European Rocket and Balloon Programmes and Related Research, June 3-7 2007, Visby, Sweden.
- [46] Cutts, J. A., Kerzhanovich, V. V., “Martian Aerobot Missions: First Two Generations” – Aerospace Conference, 2001, IEEE Proceedings. Volume 1, Issue , 2001 Page(s):1/235 - 1/242 vol.1
- [47] Voss, L., “Balloons in Planetary Research”, URL: http://www.centennialofflight.gov/essay/Lighter_than_air/Planetary/LTA16.htm [cited November 2007]
- [48] “Vega 2 Balloon” – URL: <http://nssdc.gsfc.nasa.gov/database/MasterCatalog?sc=1984-128F> [cited November 2007].
- [49] Cazaux, C., Taty, B., “Capsule ARD - Essai en vol de la phase terminale de la mission” - ESA Bulletin Nr. 89 – URL: <http://esapub.esrin.esa.it/bulletin/bullet89/cazau89.htm>
- [50] CIRA Internal Technical Document - CIRA-CF-07-0042